


Summer 7-14-2019

Natural Salinization of the Jemez River, New Mexico: An Insight From Trace Element Geochemistry

Jon K. Golla
University of New Mexico

Follow this and additional works at: https://digitalrepository.unm.edu/eps_etds

 Part of the [Geochemistry Commons](#), [Geology Commons](#), [Hydrology Commons](#), and the [Water Resource Management Commons](#)

Recommended Citation

Golla, Jon K.. "Natural Salinization of the Jemez River, New Mexico: An Insight From Trace Element Geochemistry." (2019).
https://digitalrepository.unm.edu/eps_etds/264

This Thesis is brought to you for free and open access by the Electronic Theses and Dissertations at UNM Digital Repository. It has been accepted for inclusion in Earth and Planetary Sciences ETDs by an authorized administrator of UNM Digital Repository. For more information, please contact amywinter@unm.edu.

Jon Kenneth Kabigting Golla

Candidate

Earth & Planetary Sciences

Department

This thesis is approved, and it is acceptable in quality and form for publication. *Approved by the Thesis Committee:*

Dr. Laura J. Crossey (Chair)

Dr. Karl E. Karlstrom

Dr. Shari A. Kelley

**Natural Salinization of the Jemez River, New Mexico: An Insight from Trace
Element Geochemistry**

by

Jon Kenneth Kabigting Golla

B.S., Geology, University of Puget Sound, 2017

THESIS

Submitted in Partial Fulfillment of the
Requirements for the Degree of

Master of Science

Earth & Planetary Sciences

The University of New Mexico
Albuquerque, New Mexico

July, 2019

Dedication

*To my parents, Vicky and Glenn, for their support, encouragement, and sacrifices.
They've repeatedly defied adversity with their hard work.*

Acknowledgments

I thank my committee (Shari Kelley, Karl Karlstrom, and Laura Crossey) for all their patience towards and contributions to this project. I am especially grateful to my adviser, Laura Crossey, for her steady support and guidance. She has led by example and has shown professionalism, congeniality, and the true meaning of the scientific method. Thank you to Brittany Griego and Kent Smith for assistance in the lab and in the field. None of this research would be possible without Mehdi Ali, Anna Birdsong, and Malik Yzaguirre at the Analytical Chemistry Lab. I value all the discussions with and advice from Chris McGibbon. Kate Hart, thank you for always keeping me grounded and inspired. You've always been by my side.

Financial support was provided by New Mexico EPSCoR NSF 11A-1301346 grant and awards from the Geothermal Resources Council (Graduate Scholarship), New Mexico Geological Society (Cearley Graduate Grant-in-Aid), Geological Society of America Environmental & Engineering Geology Division (Roy J. Shlemon Scholarship), New Mexico Water Resources Research Institute (Student Water Research Grant, NMWRRI-SG-2018), and Department of Earth Planetary Sciences at UNM (Alexander and Geraldine Wanek Graduate Scholarship).

Natural Salinization of the Jemez River, New Mexico: An Insight from Trace Element Geochemistry

by

Jon Kenneth Kabigting Golla

B.S., Geology, University of Puget Sound, 2017

M.S., Earth & Planetary Sciences, University of New Mexico, 2019

ABSTRACT

The Jemez River, a tributary of the Rio Grande in north-central New Mexico, receives thermal water input from the geofluids of the Valles Caldera, an active, high-temperature, liquid-dominated geothermal system. We focus on a ~50-km portion of the northern Jemez River. This research extends previous decadal work (Crossey et al., in prep., 2013) on major chemistry in the river by characterizing the response of 16 trace elements to geochemical contributions from geothermal waters (McCauley, Spence, Soda Dam, and Jemez Springs springs and San Ysidro mineral waters), an area with copious hydrothermal degassing (Hummingbird), and two major tributaries (Rio San Antonio and Rio Guadalupe) during a low-flow event (~425 L/s).

The greatest known loading (as much as 10^1 concentration increase) of trace elements to the Jemez River is from Soda Dam ([TDS] = 4700 ppm). Seventy-five percent of analyzed trace elements are coupled with major ions and resemble mostly conservative downstream behavior. Correspondent to their inherently low ionic potential, the alkali (Li, Rb, Cs) and alkali earth (Sr, Ba) metals remain abundantly dissolved. The relative non-reactivity of some transition metals (Fe, Ni, Co, U, V, Cu, Pb), which are sensitive to redox changes and susceptible to sorption, is facilitated by transport as complexed species (predominantly as $\text{Fe}(\text{OH})_3^0$, HCoO_2^- , $\text{UO}_2(\text{OH})_2^0$, VO_3OH^- , CuCO_3^0 , PbCO_3^0). There is no common sink

for the latter 25% (As, Al, Mo, Mn), as each is potentially scavenged at different sections of the river by different processes, like oxidation-enhanced adsorption and co-precipitation. The inflowing H₂S and CO₂ gases at Hummingbird impart unique physiochemical conditions that allow some solutes to become non-conservatively solubilized (Cu, Pb, Al) and removed (U, Mo).

Contents

| | |
|---|-------------|
| List of Tables | viii |
| List of Figures | ix |
| 1 Introduction | 1 |
| 1.1 Overview | 1 |
| 1.2 Site Description | 2 |
| 2 Methods | 8 |
| 2.1 Sample Collection | 8 |
| 2.2 Analytical methods | 9 |
| 2.3 Geochemical modeling | 10 |
| 3 Results & Discussion | 11 |
| 3.1 Major solutes | 17 |
| 3.2 Conservative trace elements | 17 |
| 3.3 Non-conservative trace elements | 23 |
| 3.3.1 Arsenic | 24 |
| 3.3.2 Molybdenum | 27 |
| 3.3.3 Aluminum | 29 |
| 3.3.4 Manganese | 31 |
| 4 Summary & Conclusions | 33 |
| References | 35 |
| A Field Photos | 50 |
| B Spatial Series Data | 50 |

List of Tables

| | | |
|---|--|----|
| 1 | Field parameters (from Oakton meter) and major-solute chemistry data (reported in mg/L). | 15 |
| 2 | Trace element data reported in $\mu\text{g/L}$. Cells with 'n.d.' are nondetects. . . . | 16 |

List of Figures

| | | |
|---|---|----|
| 1 | Map of study area, with outline of Jemez River and tributaries and reported sampling and survey sites. | 3 |
| 2 | Zoomed-in maps of key Jemez River junctions, highlighting the Battleship Rock confluence (a), the Hummingbird site (b), the outflow thermal spring seeps (c), the Guadalupe confluence (d), and the Guadalupe-to-San-Ysidro section. The colored (teal) polygon is a Stiff diagram (Stiff, 1951). | 5 |
| 3 | Spatial profiles of physiochemical parameters recorded by the Oakton (in orange) and YSI (in blue) meters. | 10 |
| 4 | A hydrograph (black lines) of the Jemez River near Jemez Springs, including mean daily statistics (orange 'x'), for the 2018 flow year. The red-rimmed yellow dot denotes the sampling campaign of this study. Data are obtained from online National Water Information System database (USGS, 2019). | 11 |
| 5 | A dot plot showing logarithmic distribution of analyzed solute suite. | 13 |
| 6 | A downstream plot of major-solute chemistry with marked known inflows (gray dashed) and the EPA MCL for total dissolved solids (red solid). | 14 |
| 7 | A downstream plot of trace elements that behave like TDS or major solutes, with marked known inflows. | 18 |
| 8 | Results of inorganic speciation modeling with Phreeqc. Any species contributing to ≤ 0.01 % are not included. | 20 |
| 9 | Saturation index of Jemez River waters with respect to Fe, Ni, U, Cu, Pb, Al, and Mn phases. The dashed line (Saturation Index = 0) denotes equilibrium. | 23 |

| | | |
|----|---|----|
| 10 | Subplots of arsenic downstream profile and spatial surveys of physiochemical parameters. The term, $\Delta\mu M_{\text{inflow-river}}$, is the difference in concentration between a known inflow and the preceding river sample. The line connected with 'x' markers denotes $\text{pH}_{\text{Oakton}}$ | 25 |
| 11 | A Pourbaix (Eh-pH) diagram for aqueous arsenic species with Jemez River waters plotted. | 26 |
| 12 | Subplots of molybdenum downstream profile and spatial surveys of physiochemical parameters. The term, $\Delta\mu M_{\text{inflow-river}}$, is the difference in concentration between a known inflow and the preceding river sample. The line connected with 'x' markers denotes $\text{pH}_{\text{Oakton}}$ | 28 |
| 13 | Subplots of aluminum downstream profile and spatial surveys of physiochemical parameters. The term, $\Delta\mu M_{\text{inflow-river}}$, is the difference in concentration between a known inflow and the preceding river sample. The line connected with 'x' markers denotes $\text{pH}_{\text{Oakton}}$ | 30 |
| 14 | Subplots of manganese downstream profile and spatial surveys of physiochemical parameters. The term, $\Delta\mu M_{\text{inflow-river}}$, is the difference in concentration between a known inflow and the preceding river sample. The line connected with 'x' markers denotes $\text{pH}_{\text{Oakton}}$ | 31 |

1 Introduction

1.1 Overview

In contrast to the addition of major solutes via equilibrium reactions, trace element signatures in aqueous systems are more often associated to secondary removal processes. The background abundance of dissolved trace elements in river waters is usually low due to local in-stream transport mechanisms, such as co-precipitation and adsorption reactions (Gibbs, 1973). These processes may be enhanced by unique in-situ physiochemical conditions, exposure to sunlight (Fuller and Davis, 1989; Shiller et al., 2006), microbiota (Kirk et al., 2004; Rittle et al., 1995), and hydrodynamic constraints. However, high concentrations of these solutes may still be retained when there is consistent and prolific saline input into the aqueous system. Some well-documented instances of elevated riverine trace element concentrations are anthropogenically related, namely, from cases of continuous influx of acidic runoff that leach heavy metals from rocks in abandoned mine sites (Johnson and Hallberg, 2005; Nieto et al., 2007) and poor management of industrial wastewater effluents (Mapanda et al., 2005; Mohiuddin et al., 2010). This study seeks to investigate similar, but geogenic, occurrence of trace element salinization of surface waters in the southwestern United States, where deeply-derived fluids have been shown to influence hydrologic basins at local to regional scales (Crossey et al., 2015, 2006, 2009; Kirk et al., 2009; Newell et al., 2005; Williams et al., 2013).

We focus on the Jemez River (JR) of the Jemez Watershed in north-central New Mexico, which houses the Valles Caldera (VC), an active liquid-dominated, high-temperature (≤ 300 °C) geothermal system (Goff and Grigsby, 1982). Highly mineralized geothermal systems usually have a significant hydrologic and environmental footprint. Subsurface processes, such as mixing with magmatically influenced fluids and water-rock interactions at elevated temperatures, enrich ascending and laterally-flowing geothermal waters with major and trace elements (Bau, 1991; Hedenquist and Lowenstern, 1994; Henley and Ellis,

1983; Kaasalainen and Stefánsson, 2012). The proximity of the JR to the saline surface features of the VC system poses societal and environmental concerns, since water from the JR is used by stakeholders, including the native Jemez and Zia Pueblos, for domestic, recreational, and irrigational uses. Particularly, a designated use of the JR is to host coldwater aquatic life (New Mexico Environment Department, 2016), which makes drinking water standards more considerably important due to potential of bioaccumulation of potentially harmful dissolved substances. Previous studies have examined the geochemical response of JR water to the solute contributions of the VC (Crossey et al., 2013; Hansson, 2016; Purtymun et al., 1974; Reid et al., 2003; Sherson et al., 2009; Trainer, 1978). Except for Hansson and Reid et al., these past investigations only concentrate on major chemistry and/or do not discuss enhancement of salinization during low discharge. This work emphasizes characterization of hydrogeochemical behavior during low-flow conditions, as there is often an accompanied degradation in water quality without the natural ‘flushing’ mechanism during high-discharge periods. The first part of this series compiles and highlights the longitudinal patterns of major-solute chemistry salinization over a decadal span (Crossey et al., in prep., 2013). This work focuses on a snapshot of downstream trace element signatures in the JR during a low-flow event from 2018.

1.2 Site Description

The study area (Figure 1) is centered within the Jemez Mountains, which overlies the intersection between two prominent geologic features, the Rio Grande Rift and Jemez Lineament. Miocene-to-present extension has developed a principal structural regime that trends northeast (Goff, 2009; Goff et al., 2011). Accompanied by complex and episodic volcanic activity as early as ~16 Ma (Gardner et al., 1986; Kelley et al., 2013), the evolution of the local volcanic deposits is highlighted by the development and collapse of the initial 1.651-Ma Toledo structure (Izett and Obradovich, 1994) and the smaller 1.265-Ma Valles caldera (Phillips et al., 2007), inception of Redondo Peak by uplift-induced reemergence of

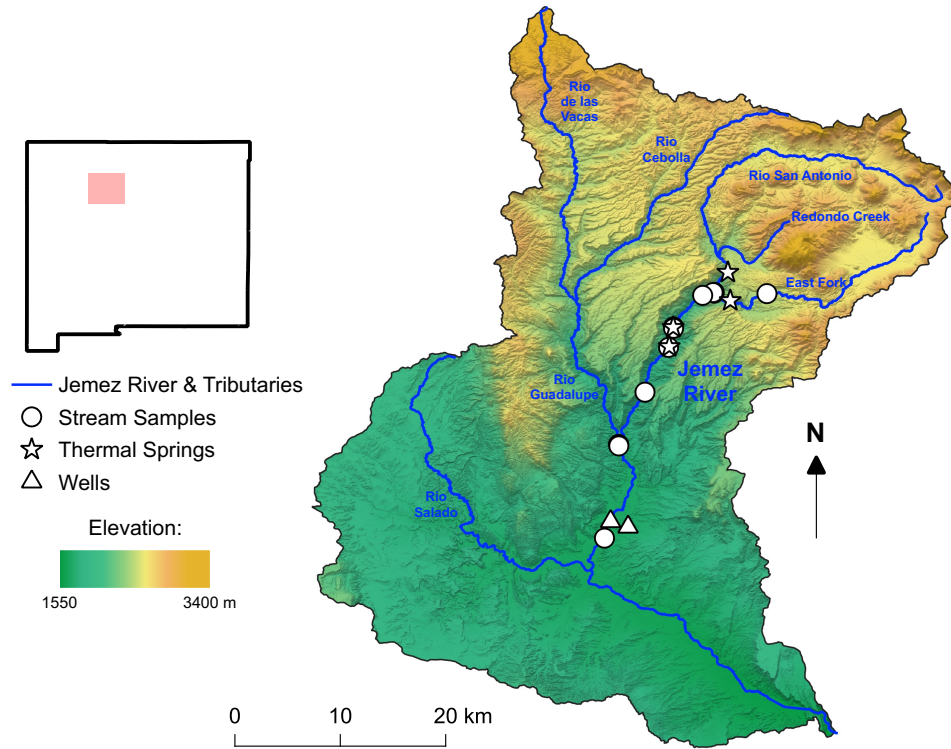


Figure 1: Map of study area, with outline of Jemez River and tributaries and reported sampling and survey sites.

the Valles Caldera floor (Phillips et al., 2007), and post-resurgence rhyolitic volcanism that had been concentrated within the ring fracture zone (Phillips et al., 2007; Spell and Harrison, 1993). Zimmerer et al. (2016) have since reported refined ages of the latest pulses of eruptive activity at 74.4 and 68.3 ka. The current VC geothermal system is probably related to this more recent volcanic activity. Modern (Tertiary-Quaternary) caldera fill generally consists of multimodal lava flows, pyroclastics, and some alluvial and lacustrine units (Goff, 2009; Goff et al., 2011). In the southwestern Jemez Mountains, older prevolcanics are exposed and are made up of Precambrian granitic gneiss and Paleozoic and Mesozoic sediments, which house the regional principal aquifers (Connell, 2011).

The ~80-km JR (Figure 1) is a major tributary to the Rio Grande. Its semiarid catchment receives most precipitation from heavy monsoonal rain between July and September, while the amount of snowfall in the winter is more variable interannually. The base flow

of the JR is regulated by a mixture of this alpine precipitation and shallow groundwater. The complex geologic history of the Jemez Mountains has created discrete subsurface flow paths (Goff et al., 1981, 1988; Trainer et al., 2000). These different fracture networks increase susceptibility of the JR to diffuse thermal water input. Along the western caldera moat, meteoric waters heated by elevated background geothermal gradient issue from fractured rhyolite (Goff et al., 1981; Trainer et al., 2000). Along the periphery of the system, the VC hydrothermal outflow plume exists as a distal expression of the deep geothermal reservoir fluids and is globally one of the few to extend to ≥ 20 km (Goff et al., 1988). Others have recently demonstrated the influence of this system using trace element and other geochemical indicators as far as south of San Ysidro (McGibbon et al., 2018), where our study reach terminates. These outflow fluids travel laterally southward, following the flow of the JR, and ascend to various sites at the surface through the Jemez Fault Zone. To assess the geochemical influence of these thermal seeps and the major tributaries of the JR, we focus on specific junctions along-stream.

The upper JR, which generally traces along State Highway NM-4, is formed by the confluence of the East Fork headwaters and Rio San Antonio (SA), the longest headwater tributary (Figure 2a). Both waters share the same Na-Ca-HCO₃ affinity, which is inherited by the upper JR. Thermal meteoric waters, Spence (SPNC) and McCauley (MCLY) springs, each occur along the reaches of these tributaries and could be providing input via mixing. Further downstream, a section of the JR at Hummingbird (HBRD) and the adjacent NM-4 are intersected by faults with upwelling hydrothermal gaseous CO₂ (Rahilly and Fischer, pers. comm.). Using similar methods, Smith (2016) showed a high CO₂ flux in association with faults at Sulphur Springs (Goff et al., 1985) in the caldera and at an outflow thermal spring downstream. The presence of H₂S is also apparent, which is evidenced by a potent ‘rotten-egg’ stench and yellow-white sulfur coatings streamside (Figure 2b; Appendix A). These gases appear to have no detectable influence on riverine major solute chemistry under the flow conditions sampled for this study, since there is no compositional change

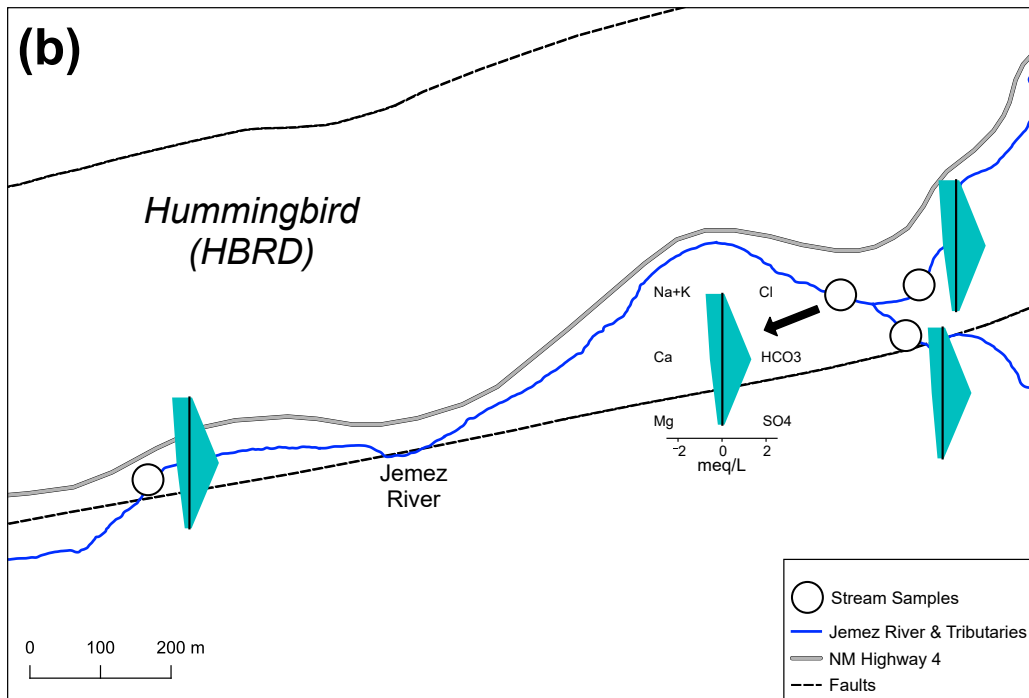
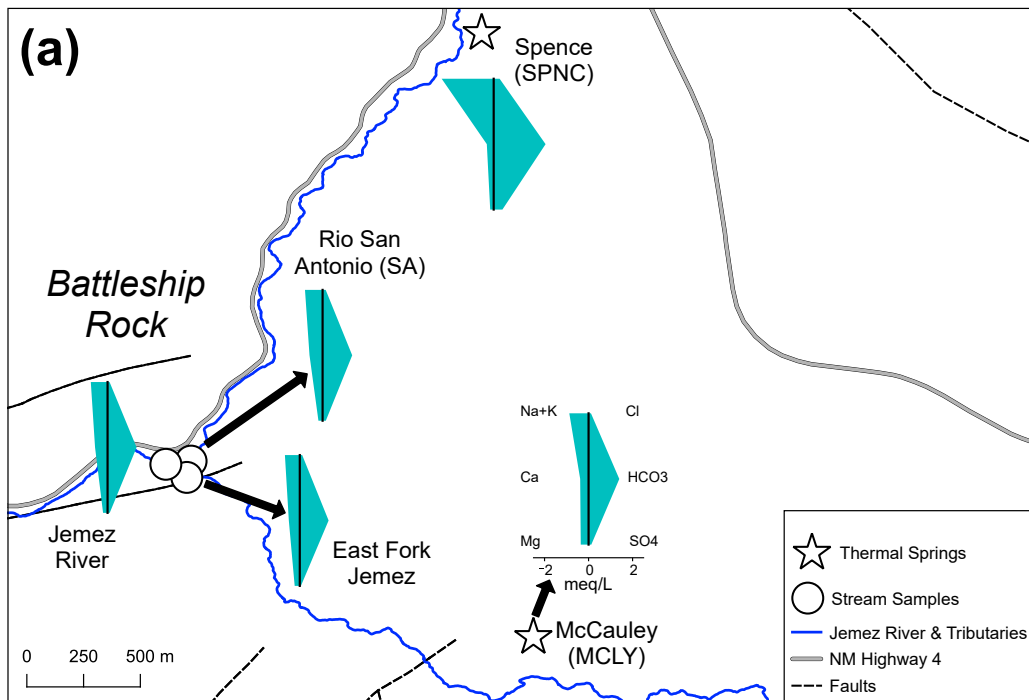


Figure 2: Zoomed-in maps of key Jemez River junctions, highlighting the BattleSHIP Rock confluence (a), the Hummingbird site (b), the outflow thermal spring seeps (c), the Guadalupe confluence (d), and the Guadalupe-to-San-Ysidro section. The colored (teal) polygon is a Stiff diagram (Stiff, 1951).

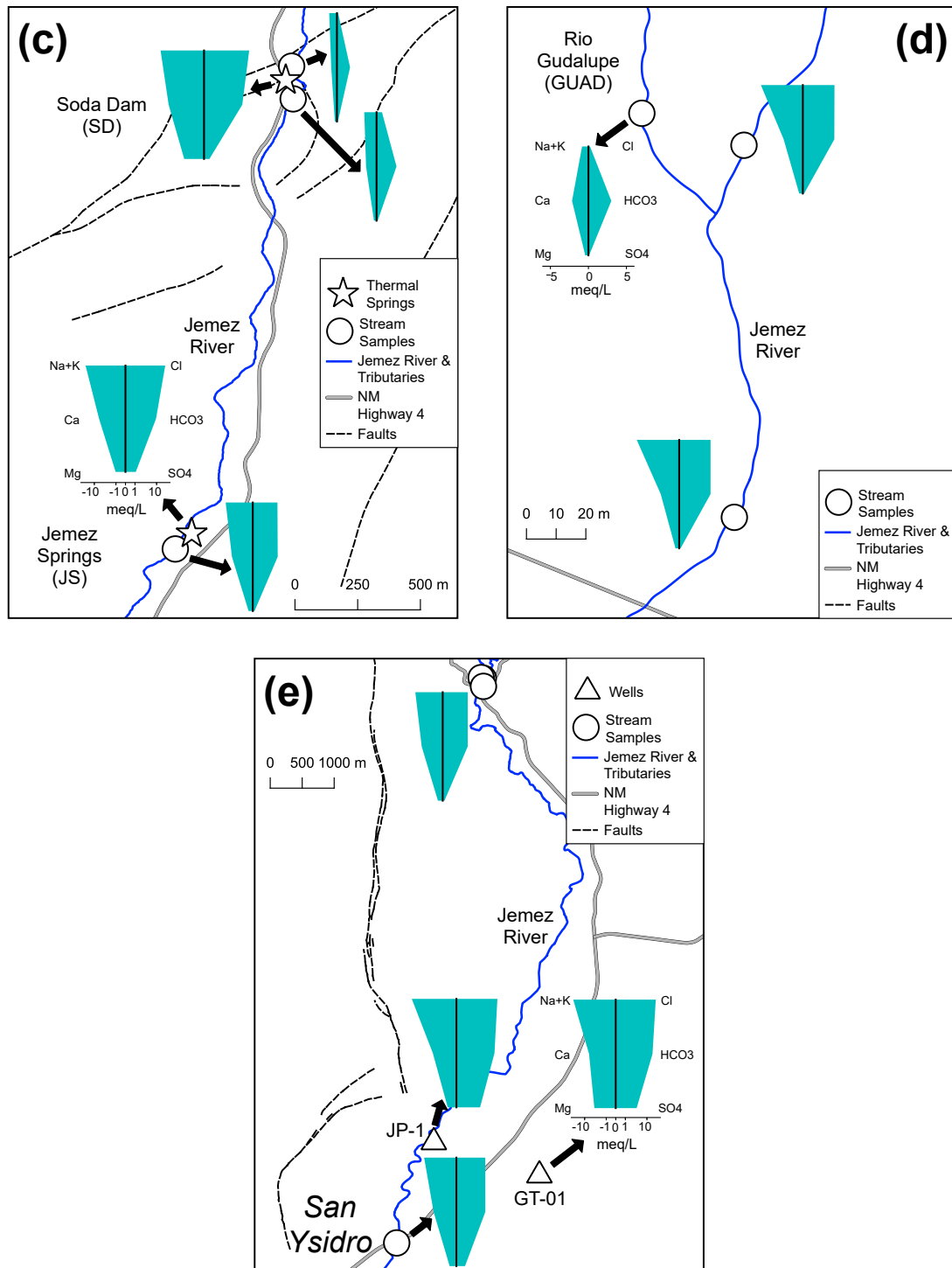


Figure 2 (cont.): Zoomed-in maps of key Jemez River junctions, highlighting the Battleship Rock confluence (a), the Hummingbird site (b), the outflow thermal spring seeps (c), the Guadalupe confluence (d), and the Guadalupe-to-San-Ysidro section. The colored (teal) polygon is a Stiff diagram (Stiff, 1951).

relative to upstream conditions. The most significant observed changes in water chemistry occur within the Cañon de San Diego region (Figure 2c). Here, Soda Dam (SD) and Jemez Springs (JS) hot springs apparently issue from discrete flow paths within the Jemez Fault Zone (Goff et al., 1981), and emerge as warm, mineralized, and CO₂-charged fluids (as demonstrated by massive and terraced travertine deposits; Appendix A). River waters mixing with these thermal waters are imparted with a Na-Cl-HCO₃ signature and an order-of-magnitude increase in total dissolved solids (TDS) from above to below spring seepage. The only other tributary to the JR is Rio Guadalupe (GUAD), with a confluence about thirteen kilometers downstream from JS (Figure 2d). The JR below GUAD does not acquire the inflowing Ca-HCO₃ composition but is diluted by the relatively lower TDS of the GUAD. From the GUAD triad to San Ysidro, there is another significant concentration increase in all major solutes (Figure 2e). The contributing saline end-member likely belongs to the San Ysidro mineral waters (Goff et al., 1981, 1988), which contain a VC outflow component and circulate within Mesozoic and Paleozoic strata (McGibbon et al., 2018). Our representative waters are from the JP-1 and GT-01 wells, which were drilled for geothermal exploration in the Jemez Pueblo through a U.S. Department of Energy initiative (Albrecht et al., 2015).

2 Methods

2.1 Sample Collection

The JR and its known inflows were sampled from a total of fifteen sites in August 25th, 2018. Samples were obtained from tributaries (SA, GUAD) and springs (SD, JS) and their accompanying above- and below-JR sites, with four additional locations from East Fork furthest upstream, the HBRD junction, the JR Spanish Queen fishing grounds between JS and the GUAD tributary, and at the intersection of the JR and NM-4 at the village of San Ysidro (JRSY). Approximately fifteen kilometers separate JRSY from the last river sampling site, the GUAD tributary (the intervening area is the Jemez Pueblo). We were unable to collect a sufficient sample volume from JS, as there was nearly no runoff from the spout of the enclosed JS bathhouse well at the time of the campaign. Thus, an older JS sample from 2017 is substituted. Potential thermal meteoric water inflows, SPNC and MCLY springs, were also sampled in 2017. For the San Ysidro end-members, we use a JP-1 sample, which has data partially reported in [McGibbon et al. \(2018\)](#), and obtain unpublished data for the GT-01 well from the [Albrecht et al. \(2015\)](#) effort. [Goff et al. \(1981\)](#) report that the mineral springs derived from the VC outflow fluids have remained relatively chemostatic for over half a century and any input from surface hydrology is negligible. Although there is seasonality in the geochemistry of the thermal meteoric waters ([Vuataz and Goff, 1986](#)), SPNC and MCLY were sampled during early winter, avoiding dilution from snowmelt recharge.

In the field, we follow water sampling protocols defined by the U.S. Geological Survey National Field Manual for the Collection of Water-Quality Data ([Wilde, 2006](#)). At each site, a pair of treated (0.45- μ m-filtered and HNO₃-acidified) and raw (and without headspace) samples was collected in Nalgene high-density polyethylene bottles for cation measurements and analyses of anions, respectively. The temperature, pH, TDS, and specific conductance of these waters are recorded with an Oakton Waterproof pH/CON 300 meter. To complement these stations of discretely sampled water chemistry, a spatial sur-

vey of an extended suite of physiochemical parameters, which includes temperature, pH, TDS, specific conductivity, oxidation-reduction potential (ORP), dissolved oxygen, and turbidity, was synoptically conducted using a YSI ProDSS multiparameter water quality meter during the campaign (Figure 3). The Ag/AgCl reference ORP electrode (in 4 M KCl) was calibrated with a YSI 3682 ZoBell Solution and its measured potentials are converted to and reported as Eh in volts (V)

$$Eh = E_{\text{field}} + \underbrace{(-0.001 * T + 0.224)}_{E_{\text{ref}}}, \quad (1)$$

where E_{field} is the in-situ potential and E_{ref} is the potential of the given reference electrode, which is calculated with a temperature-dependent (T in °C) linear expression derived from standard values (Nordstrom and Wilde, 2005, their Table 6.5-2). We employed regular 1-km spacing throughout the upper JR reach and finer 50-m frequency around sites with grab samples. Any gaps in these spatial series records are along restricted residential and reservation areas.

2.2 Analytical methods

Total alkalinity (expressed as HCO_3) was measured via potentiometric acid-neutralization titration (Dickson, 1981; Gran, 1952) correspondent to Standard Method 2320 (Association et al., 2018). All instrumental analyses were done at the Analytical Geochemistry Laboratory at the University of New Mexico (UNM). Major solute chemistry was analyzed using a Perkin Elmer Avio 500 inductively coupled optical emission spectrometer (Na, K, Mg, Ca, Si) and a Dionex ICS-1100 ion chromatograph (Cl, SO_4 , F) similar to methods disclosed in Environmental Protection Agency (EPA) 200.7 and 300.0 (Pfaff, 1993), respectively. Sixteen trace elements (Fe, Li, U, Sr, Rb, Ba, Co, Pb, Cu, Ni, V, Cs, Mo, Mn, As, Al) were analyzed with a Perkin Elmer NexION 300D inductively coupled plasma mass spectrometer following EPA method 200.8. As a QA/QC protocol, a continuing calibration

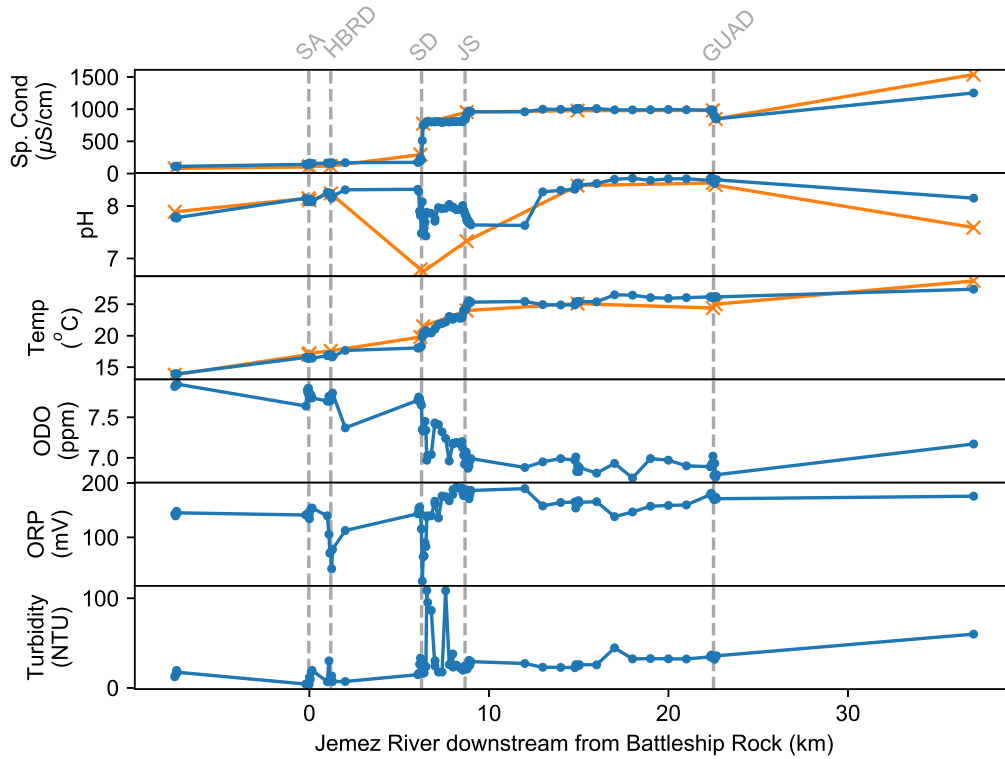


Figure 3: Spatial profiles of physiochemical parameters recorded by the Oakton (in orange) and YSI (in blue) meters.

verification solution, prepared from a PlasmaCAL SCP33MS reference reagent, was analyzed three times (each at the beginning, midpoint, and end of analysis) to ensure accuracy within $\leq 5\%$. The response of an internal indium standard for drift assessment every sample showed a range of 97% - 120% recovery. Replicates for 10% of total unknown samples were in good agreement within $\leq 5\%$ of each other.

2.3 Geochemical modeling

We use Phreeqc (Parkhurst and Appelo, 2013), an equilibrium-based geochemical program maintained by the U.S. Geological Survey, and the 11n1 .dat thermodynamic database (Johnson et al., 2000) to compute aqueous speciation and mineral saturation indices. Model input consisted of major and trace solute chemistry and Eh measured by the YSI meter.

3 Results & Discussion

All data are presented in [Table 1](#) and [Table 2](#). Spatial series of physiochemical parameters are tabulated in [Appendix B](#). The data reported are obtained during a ~ 425 L/s event on the given sampling date. This discharge is estimated from a United States Geological Survey stream gauging station (unit #08324000) below the confluence at GUAD ([USGS, 2019](#)). The flow conditions during our campaign are about 25% weaker than the mean daily value ([Figure 4](#)) and is almost just half of the reported flow (~ 963 L/s) in the loading assessment by [Dyer \(2007\)](#), during which some major elements and heavy metals, like As, were found to have been exceeding EPA drinking water standards.

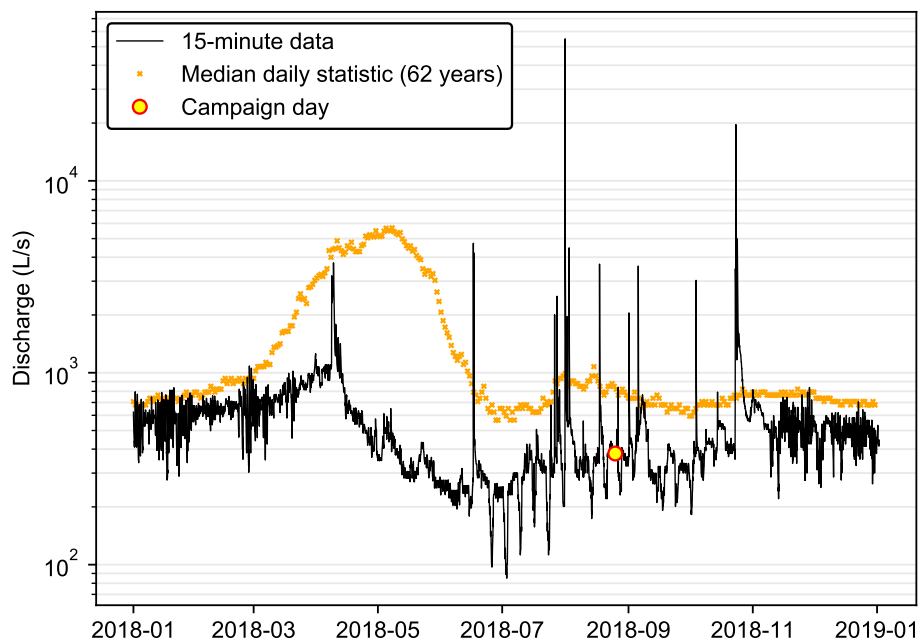


Figure 4: A hydrograph (black lines) of the Jemez River near Jemez Springs, including mean daily statistics (orange 'x'), for the 2018 flow year. The red-rimmed yellow dot denotes the sampling campaign of this study. Data are obtained from online National Water Information System database ([USGS, 2019](#)).

The distribution of detected solute concentrations is shown by [Figure 5](#). Some trace elements, like Li and Sr, are within the lower range of major-solute abundance, measur-

ing up to as much as ~ 1 ppm. Except for V and Al, which are the most enriched in river samples, the greatest measured values are in springs. The thermal meteoric waters, SPNC and MCLY springs, are generally depleted in most solutes, often below or middling within the range of river concentrations. However, these waters contain the most Mo, which may be a consequence of their relatively long residence times (Dondanville, 1971; Goff et al., 1981; Vuataz and Goff, 1986). Notably, within fractured and highly-altered Quaternary tuff from a core extracted in the dry-steam region of the caldera, Hulen et al. (1987) found shallow molybdenite deposits, which are hypothesized to have formed from prior existence of a liquid-dominated system or leakage of such high-temperature waters via favorable conduits of the Sulphur Creek fault network. This remnant mineralization may have also occurred within fractured Quaternary moat rhyolite that hosts the thermal meteoric waters, which are located just outside the caldera ring fracture and near the northeastern terminus of the Jemez Fault Zone. The latter springs that account for most of the high solute concentrations are surface expressions of the saline VC outflow plume and each has undergone a unique flow path, which is reflected by different solute abundances.

Although the origins of the geochemical differences among spring groups in Cañon de San Diego have not been fully determined (Goff et al., 1981, 1988; McGibbon et al., 2018), the trace element data provide additional constraints in identifying the correspondent lithology these thermal waters have significantly interacted with. Generally, JS is more enriched in heavy metals while SD contains more alkali and alkaline-earth metals. The JS waters were likely in communication with the local Cu-rich (Elston, 1967; McLemore, 1996) azurite and malachite deposits of the Permian Abo Formation sandstone (Kelley et al., 2003, 2007), given the maximum concentrations found in this spring. Alongside Cu, Ag, Au, and U have also been extracted from the Abo (Elston, 1967; McLemore, 1996). It's possible the fluids that formed the ore minerals also provided sources of mineralized Ni and Co, the other trace metals most abundantly found in JS. The SD waters show the greatest extent of interaction with the Pennsylvanian Madera limestone, which is reflected by the

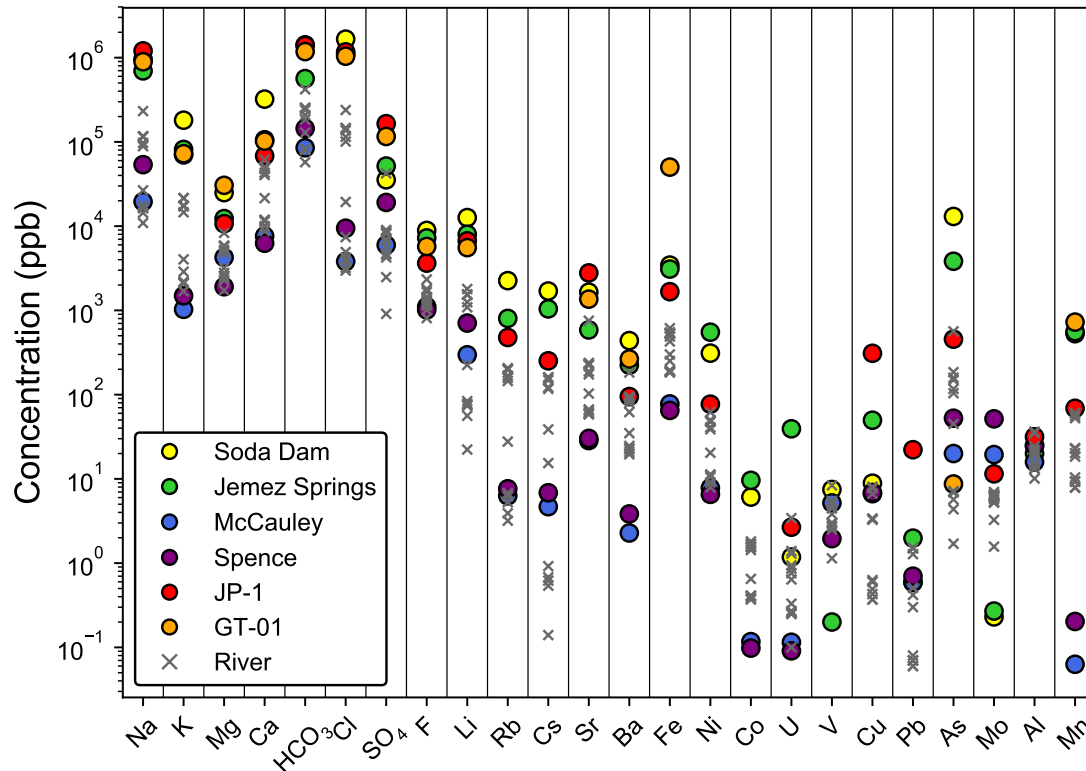


Figure 5: A dot plot showing logarithmic distribution of analyzed solute suite.

highest HCO₃ concentrations and abundance of some alkali and alkaline-earth metals that are often incorporated as constituents of carbonates (Graf, 1962; Heier and Adams, 1964; Nesbitt et al., 1980).

The thermal waters in the Jemez Pueblo area are still derived from the VC outflow, but their geochemical composition has been significantly altered by interaction with lower Permian rocks. Dissolution of evaporites in the Yeso Formation is demonstrated by a loss of a radiogenic signature, or lower ⁸⁷Sr/⁸⁶Sr ratios denoting a shift to a marine end-member (McGibbon et al., 2018), and elevated SO₄, HCO₃, and Sr concentrations in the representative well waters (Figure 5). High Cu and Pb concentrations in the JP-01 well waters may originate from interaction with the underlying Abo Formation. Furthermore, the depleted signatures of Rb, Cs, and Ba support uptake into Na- and K-bearing minerals like those in the arkosic sandstones and interbedded clays of the Abo (Goff et al., 2011).

The GT-01 well contains almost 100 ppm of Fe, which may be associated to widespread occurrence of hematite (Albrecht et al., 2015) or may originate from well contamination.

We further interpret how these spring sources influence the availability and behavior of trace elements in the JR with downstream distance-concentration profiles, where the confluence at Battleship Rock (Figures 2 and 6) is used as the datum for the JR study reach.

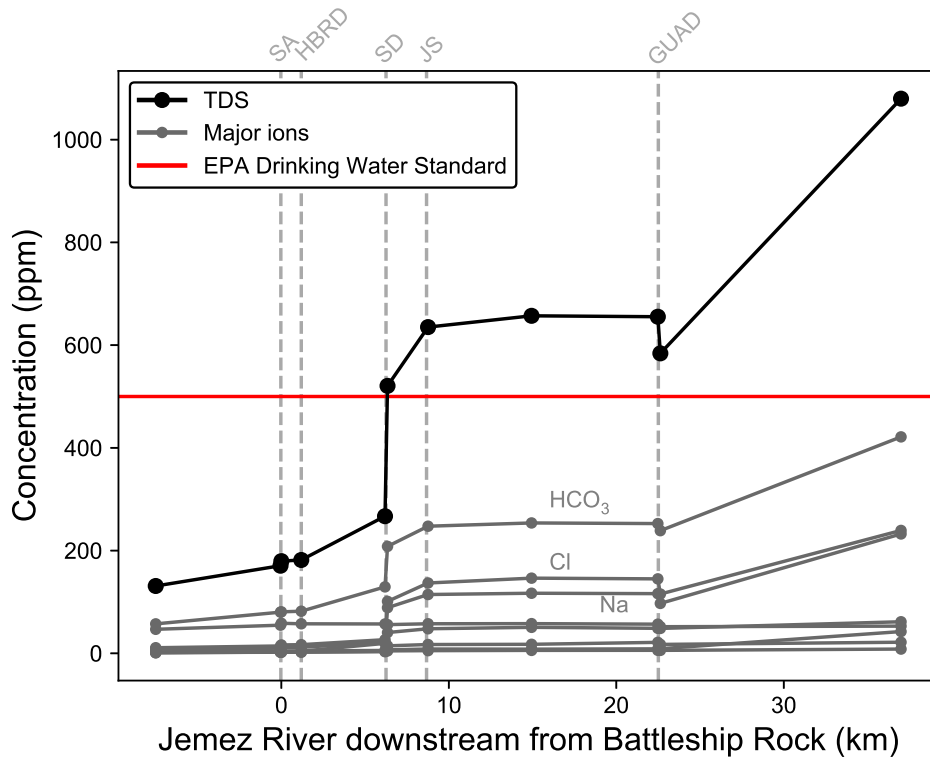


Figure 6: A downstream plot of major-solute chemistry with marked known inflows (gray dashed) and the EPA MCL for total dissolved solids (red solid).

Table 1: Field parameters (from Oakton meter) and major-solute chemistry data (reported in mg/L).

| Sample | Date | Lat (N) | Lon (W) | pH | Temp. (°C) | Sp. Cond. (µS/cm) | TDS (mg/L) | Na | K | Mg | Ca | HCO ₃ | Cl | SO ₄ | F | SiO ₂ | CBE (%) |
|--------|------------|----------|------------|------|------------|-------------------|------------|------|------|------|------|------------------|------|-----------------|------|------------------|---------|
| MCLY | 11/10/2017 | 35.82002 | -106.62725 | 7.40 | 32.7 | 174 | 87.0 | 19.5 | 1.03 | 4.26 | 7.62 | 85.2 | 3.81 | 5.97 | 1.11 | 53.8 | -0.66 |
| EFHJ | 8/25/2018 | 35.82735 | -106.58902 | 7.89 | 13.8 | 80 | 40.1 | 10.9 | 1.69 | 1.73 | 8.73 | 57.4 | 2.97 | 0.91 | 1.28 | 46.8 | 2.5 |
| SPNC | 11/10/2017 | 35.84946 | -106.62977 | 8.07 | 34.4 | 314 | 157 | 53.7 | 1.49 | 1.91 | 6.27 | 144 | 9.45 | 19.1 | 1.01 | 62.8 | -3.2 |
| SAABR | 8/25/2018 | 35.82860 | -106.64394 | 8.03 | 16.66 | 121 | 58.5 | 17.2 | 2.12 | 2.28 | 11.9 | 82.4 | 4.93 | 7.05 | 1.79 | 61.0 | -1.5 |
| EFABR | 8/25/2018 | 35.82781 | -106.64415 | 8.15 | 17.0 | 101 | 52.6 | 14.4 | 2.10 | 2.79 | 9.99 | 80.2 | 3.86 | 2.48 | 1.01 | 54.8 | -2.4 |
| JRBBR | 8/25/2018 | 35.82844 | -106.64517 | 8.11 | 17.2 | 113 | 56.2 | 16.3 | 2.10 | 2.46 | 11.4 | 80.8 | 3.20 | 4.70 | 1.42 | 58.5 | 0.8 |
| JRHHB | 8/25/2018 | 35.82554 | -106.65603 | 8.24 | 17.6 | 116 | 58.0 | 16.9 | 2.20 | 2.57 | 11.8 | 82.0 | 4.21 | 4.60 | 1.43 | 57.5 | 1.0 |
| JRASD | 8/25/2018 | 35.79270 | -106.68645 | 6.79 | 19.8 | 294 | 153 | 26.6 | 4.03 | 3.20 | 21.5 | 129 | 19.4 | 5.65 | 1.35 | 57.2 | -3.6 |
| JRBSD | 8/25/2018 | 35.79126 | -106.68638 | 6.75 | 21.5 | 775 | 387 | 88.9 | 14.6 | 4.74 | 40.5 | 208 | 101 | 6.77 | 1.14 | 55.9 | 1.9 |
| SDS | 8/25/2018 | 35.79209 | -106.68671 | 6.30 | 45.6 | 6560 | 3200 | 961 | 181 | 25.0 | 322 | 1420 | 1658 | 35.5 | 8.90 | 46.2 | -3.6 |
| JRJS | 8/25/2018 | 35.77141 | -106.69158 | 7.33 | 24.0 | 956 | 481 | 115 | 17.2 | 5.21 | 47.9 | 247 | 137 | 8.42 | 1.65 | 57.6 | 0.9 |
| JS | 10/14/2017 | 35.77210 | -106.69086 | 7.26 | 57.6 | 1850 | 920 | 697 | 81.4 | 12.3 | 106 | 564 | 1105 | 51.7 | 7.25 | 94.1 | -3.6 |
| JRSQ | 8/25/2018 | 35.72475 | -106.71616 | 8.39 | 25.1 | 977 | 489 | 117 | 17.6 | 5.74 | 50.6 | 254 | 146 | 8.13 | 1.76 | 57.8 | 0.5 |
| JRAG | 8/25/2018 | 35.67020 | -106.74346 | 8.44 | 24.4 | 981 | 490 | 116 | 21.4 | 5.88 | 48.7 | 253 | 145 | 8.73 | 1.41 | 56.8 | 0.6 |
| GUAD | 8/25/2018 | 35.67032 | -106.74384 | 8.07 | 24.8 | 329 | 164 | 17.6 | 2.88 | 5.03 | 43.1 | 184 | 7.41 | 4.25 | 0.81 | 33.5 | 1.4 |
| JRBQ | 8/25/2018 | 35.66882 | -106.74343 | 8.40 | 25.0 | 848 | 425 | 97.2 | 17.4 | 5.79 | 48.5 | 239 | 115 | 9.00 | 1.20 | 51.9 | 1.4 |
| JP-1 | 2/13/2016 | 35.59020 | -106.75200 | 6.20 | 58.1 | 4310 | 4083 | 1204 | 70.1 | 10.7 | 68.3 | 1392 | 1172 | 165 | 3.64 | 38.0 | -3.2 |
| GT-01 | 11/22/2013 | 35.58447 | -106.73378 | 6.71 | 45.9 | 4940 | 3434 | 893 | 72.4 | 30.5 | 102 | 1180 | 1040 | 116 | 5.74 | 54.7 | -0.7 |
| JRSY | 8/25/2018 | 35.57282 | -106.75840 | 7.59 | 28.7 | 1539 | 768 | 232 | 21.6 | 8.31 | 61.5 | 421 | 239 | 42.4 | 2.33 | 53.0 | -0.4 |

Table 2: Trace element data reported in $\mu\text{g/L}$. Cells with 'n.d.' are nondetects.

| Sample | As | Mn | Fe | Al | Cu | U | Ni | Co | Pb | Ba | Li | Mo | Rb | Sr | V | Cs |
|--------|-------|-------|-------|------|------|------|------|------|------|------|-------|------|------|------|------|------|
| MCLY | 87.9 | 2.61 | 165 | 252 | 9.34 | 4.43 | 39.5 | 1.01 | n.d. | 2.19 | 274 | 19.0 | 6.59 | 29.1 | 5.29 | 5.06 |
| EFHJ | 1.70 | 20.2 | 251 | 35.1 | 0.49 | 0.10 | 7.91 | 0.38 | 0.08 | 19.6 | 22.3 | 1.57 | 3.19 | 59.5 | 1.14 | n.d. |
| SPNC | 203 | 3.19 | 159 | 323 | 32.6 | 4.12 | 51.8 | 0.64 | n.d. | 0.88 | 0.06 | 0.78 | 0.01 | 2.55 | 0.08 | 0.01 |
| SAABR | 5.70 | 10.4 | 194 | 21.5 | 0.37 | 0.25 | 11.3 | 0.41 | 0.07 | 20.9 | 77.7 | 6.98 | 6.66 | 58.3 | 2.50 | 0.68 |
| EFABR | 7.17 | 7.88 | 188 | 24.3 | 0.43 | 0.26 | 9.03 | 0.37 | 0.06 | 24.6 | 73.7 | 5.31 | 5.28 | 66.7 | 2.94 | 0.54 |
| JRBBR | 6.90 | 9.37 | 183 | 18.8 | 0.37 | 0.27 | 10.5 | 0.41 | 0.06 | 22.5 | 75.9 | 6.51 | 6.21 | 60.7 | 2.70 | 0.62 |
| JRHB | 7.01 | 9.24 | 188 | 20.8 | 0.60 | 0.25 | 10.9 | 0.40 | 0.07 | 23.2 | 83.7 | 6.22 | 6.78 | 64 | 2.74 | 0.92 |
| JRASD | 45.0 | 23.2 | 300 | 14.7 | 0.63 | 0.33 | 20.4 | 0.65 | 0.07 | 34.9 | 225 | 6.56 | 27.7 | 103 | 3.01 | 15.4 |
| JRBSD | 564 | 60.2 | 489 | 15.3 | 6.67 | 0.64 | 38.8 | 1.43 | 1.28 | 62.0 | 1089 | 6.21 | 1.68 | 188 | 3.82 | 122 |
| SDS | 13035 | 529 | 3448 | 24.7 | 8.89 | 1.18 | 311 | 6.08 | 0.59 | 438 | 12636 | 0.23 | 2254 | 1645 | 7.48 | 1699 |
| JRJS | 185 | 52.6 | 539 | 13.2 | 7.73 | 0.76 | 47.7 | 1.68 | 1.52 | 79.4 | 1536 | 6.09 | 206 | 225 | 4.46 | 161 |
| JS | 3832 | 560 | 3094 | 20.0 | 49.7 | 39.3 | 551 | 9.61 | 1.98 | 224 | 8015 | 0.27 | 803 | 586 | 0.20 | 1042 |
| JRSQ | 159 | 18.4 | 548 | 15.0 | 7.94 | 0.86 | 49.6 | 1.69 | 1.50 | 88.0 | 1547 | 6.02 | 204 | 232 | 5.04 | 159 |
| JRAG | 150 | 7.90 | 528 | 13.3 | 8.08 | 0.94 | 48.0 | 1.55 | 1.51 | 93.8 | 1532 | 5.73 | 197 | 238 | 5.24 | 149 |
| GUAD | 4.36 | 60.7 | 428 | 36.4 | 3.38 | 3.42 | 40.9 | 1.54 | 0.42 | 88.0 | 56.1 | 3.26 | 3.91 | 174 | 5.47 | 0.14 |
| JRBQ | 117 | 22.7 | 524 | 22.4 | 3.27 | 1.30 | 49.1 | 1.58 | 0.51 | 94.5 | 1252 | 5.23 | 158 | 225 | 5.41 | 117 |
| JP-1 | 456 | 68.9 | 1668 | 31.6 | 3.10 | 2.67 | 77.1 | n.d. | 22.2 | 94.9 | 6687 | 11.5 | 477 | 2787 | n.d. | 252 |
| GT-01 | 8.70 | 726.0 | 50200 | n.d. | n.d. | n.d. | n.d. | n.d. | n.d. | 265 | 5560 | n.d. | n.d. | 1360 | n.d. | n.d. |
| JRSY | 104 | 56.1 | 614 | 10.1 | 3.36 | 1.39 | 62.0 | 1.81 | 0.30 | 183 | 1796 | 6.39 | 145 | 754 | 8.37 | 38.7 |

3.1 Major solutes

Major-ion chemistry in the JR from 2018 reflects patterns observed in sampling campaigns from the preceding decade (Figure 6) (Crossey et al., in prep., 2013; Jochems et al., 2010). Except for GUAD, there is an increase in solute concentrations at each inflow. The greatest contributions are usually at SD, where diffuse thermal seeps have been identified (Goff et al., 1981), and the flow path through SY, along which groundwaters are dissolving carbonates and evaporites (Goff et al., 1981; McGibbon et al., 2018; Trainer et al., 2000). Levels of total dissolved solids begin to exceed the EPA primary drinking water standard at JR below SD. This salinization load is maintained throughout the rest of the JR study reach, which is characteristically defined by conservative behavior, since changes in downstream concentrations only occur when mixing with inflowing waters of different geochemical compositions.

This behavior holds true for all major ions, including SO_4 , which is a solute that has been characterized to originate from multiple sources in the VC (Szynkiewicz et al., 2019b, 2012). Given the connection of the SA tributary to the intra-caldera Sulphur Creek watershed (Goff and Grigsby, 1982; Vuataz and Goff, 1986) and the influence of SPNC-like thermal waters, the JR headwater SO_4 sources are derived from oxidized H_2S in fumarolic condensates and from oxidation of S dissolved from altered rhyolite (Szynkiewicz et al., 2019b). The proportions of this combination differ seasonally, as there is more contribution from condensed geothermal steam during the winter due to greater availability of surface water (Szynkiewicz et al., 2019a). The SO_4 content in the hydrothermal outflow fluids and springs comes from Paleozoic sedimentary strata (Szynkiewicz et al., 2019b), which has also been suggested by McGibbon et al. (2018).

3.2 Conservative trace elements

The 12 of 16 measured trace elements reflect the salinization pattern of major solutes and mostly behave conservatively downstream (Figure 7). These solutes can be grouped ac-

According to their inherent chemical properties. The alkali (Li, Rb, and Cs) and alkaline-earth metals (Ba and Sr) are cations with low ionic potential, and, thus, are weakly electrostatically attracted to anions like O_2^- (Railsback, 2003). This weak bonding potential enables relatively good solubility. The rest of the elements (Fe, Ni, Co, V, U, Pb, and Cu) consists of cations with intermediate potential, which have a greater likelihood of coordinating with S and O groups and may be potentially incorporated into major oxides and hydroxides, aluminosilicates, sulfides, and carbonates (Railsback, 2003). This second group of conservatively behaving elements may also exist under variable oxidation states, some of which are insoluble forms (Brookins, 1988).

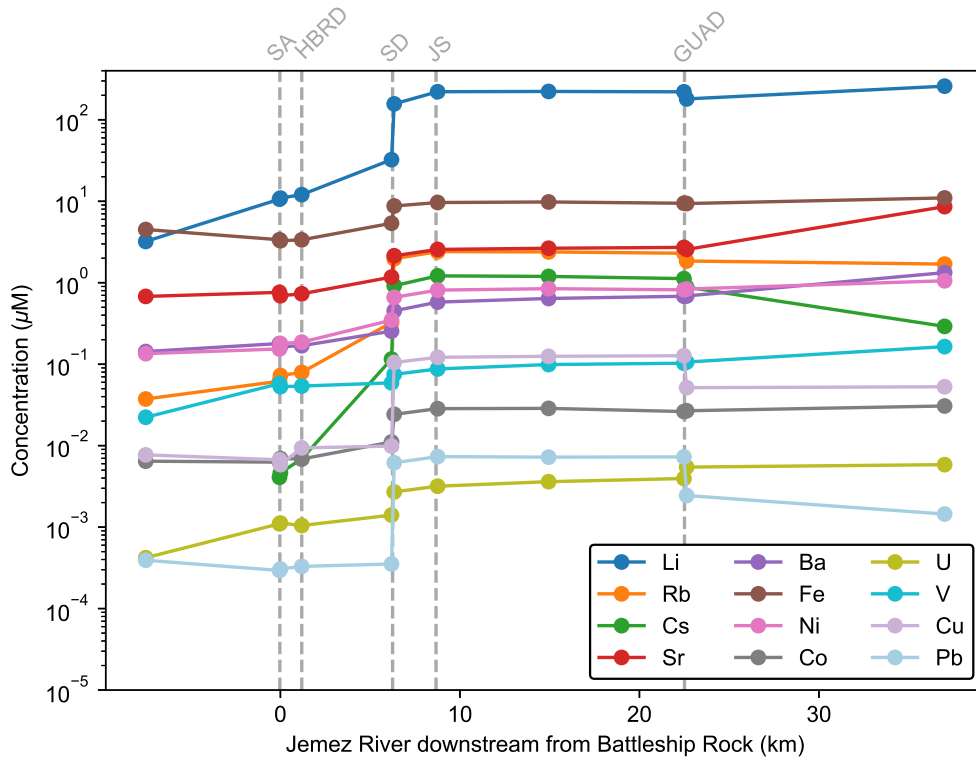


Figure 7: A downstream plot of trace elements that behave like TDS or major solutes, with marked known inflows.

The JR waters above SD likely represent background concentrations, which may be derived from a combination soil, atmospheric, or weathering contributions (Gaillardet et al., 2003) and input from the thermal meteoric waters (Figure 5). Several elements appear

more concentrated at the HBRD site, where there is no known aqueous inflow but visual fumarolic emergence. The sharp shift to reducing conditions (Figure 3) could solubilize adsorbed or suspended Cu and Pb (Davranche and Bollinger, 2000; Godtfredsen and Stone, 1994; Lin and Valentine, 2008). The source of the increase in Li, Sr, and Rb is more difficult to constrain, but may be associated to uncharacterized hyporheic exchange. The decrease in U could be caused by transformation to a U(IV) species, which would be immobile at moderate-to-high pH (Gascoyne, 1992), although no oxidation state change is suggested by speciation modeling (Figure 8). The dissolved load of all conservative metals below SD is then significantly enriched by thermal water contribution (Figure 7).

The alkali and alkaline-earth trace elements remain in solution after loading at SD, which corresponds to their aforementioned electrostatic characteristics. The transition metals behave similarly and do not react further downstream of the SD inflow. In-stream geochemistry appears to favor formation of some minerals for Fe and Ni (Figure 9). Over-saturation with respect to a mineral does not necessarily guarantee precipitation, as a solid phase will only crystallize if the kinetics are favorable. More importantly, except for Ni, which is present as a divalent ion for all of the river reach, the conservative transition metals predominantly exist downstream as hydroxyo ($\text{Fe}(\text{OH})_3^0$, $\text{UO}_2(\text{OH})_2^0$, $\text{VO}_3\text{OH}^{-2}$), oxy (HCoO_2^-), and carbonato (CuCO_3^0 , PbCO_3^0) complexes (Figure 8). The continued stability of these aqueous forms further downstream could be enhancing solubility and preventing precipitation. Although these transition metals are sensitive to changes in Eh, only Fe shows a change in oxidation state, in which Fe(II) enters the JR as a free ion and a carbonyl (FeHCO_3^+) complex (Figure 8) at the SD inflow, where Eh levels drop (Figure 3). Notably, Co may only exist in one oxidation state over the range of Eh conditions that covers natural waters (Garrels and Christ, 1965). The generally increasing turbidity trend downstream also presents potential for removal via adsorption (Figure 3). However, given the moderate dissolved SiO_2 concentration range (47-59 mg/L), it's possible that water-sediment interaction for some trace metals is minimized by potentially present silica coatings (Davis et al.,

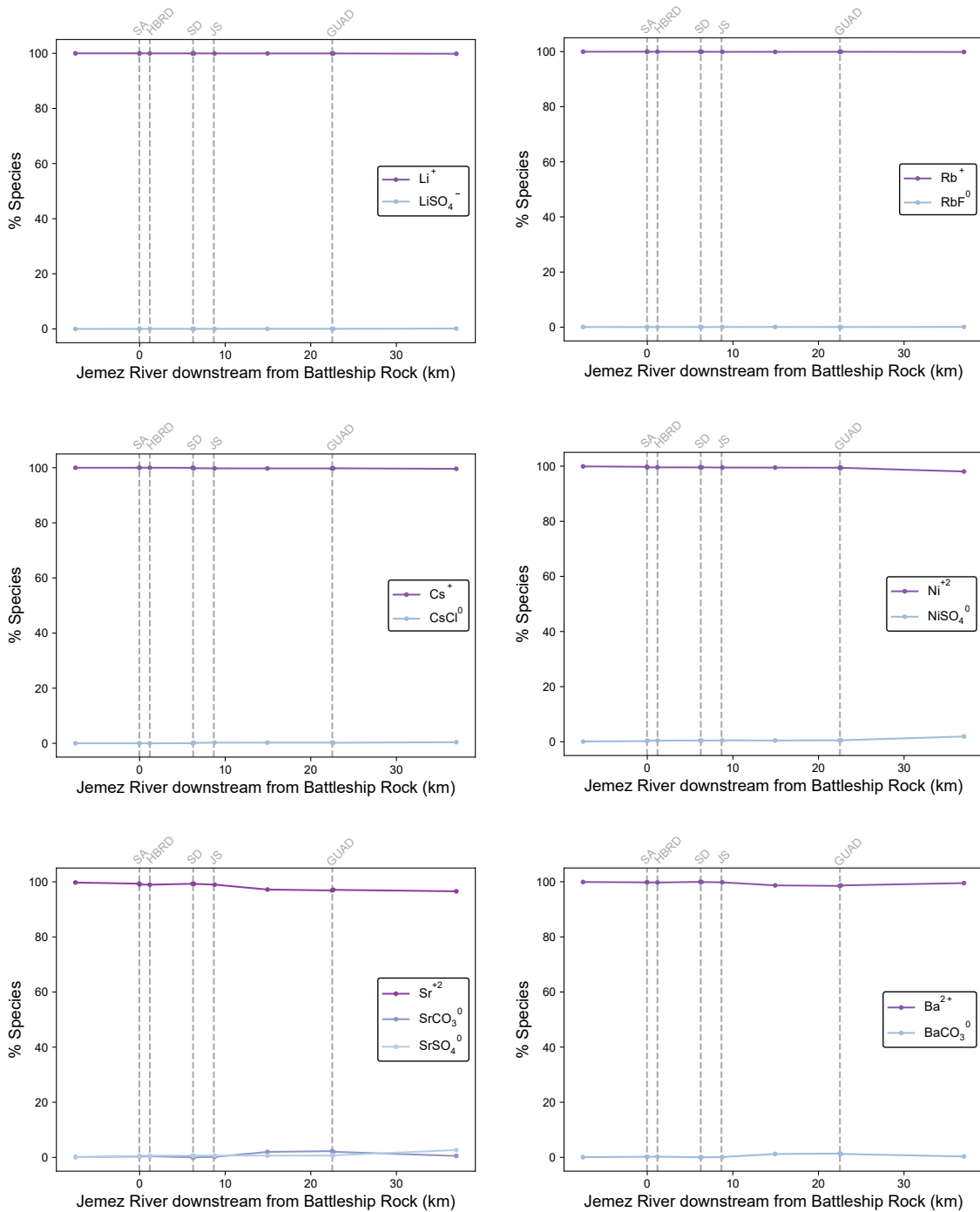


Figure 8: Results of inorganic speciation modeling with Phreeqc. Any species contributing to $\leq 0.01\%$ are not included.

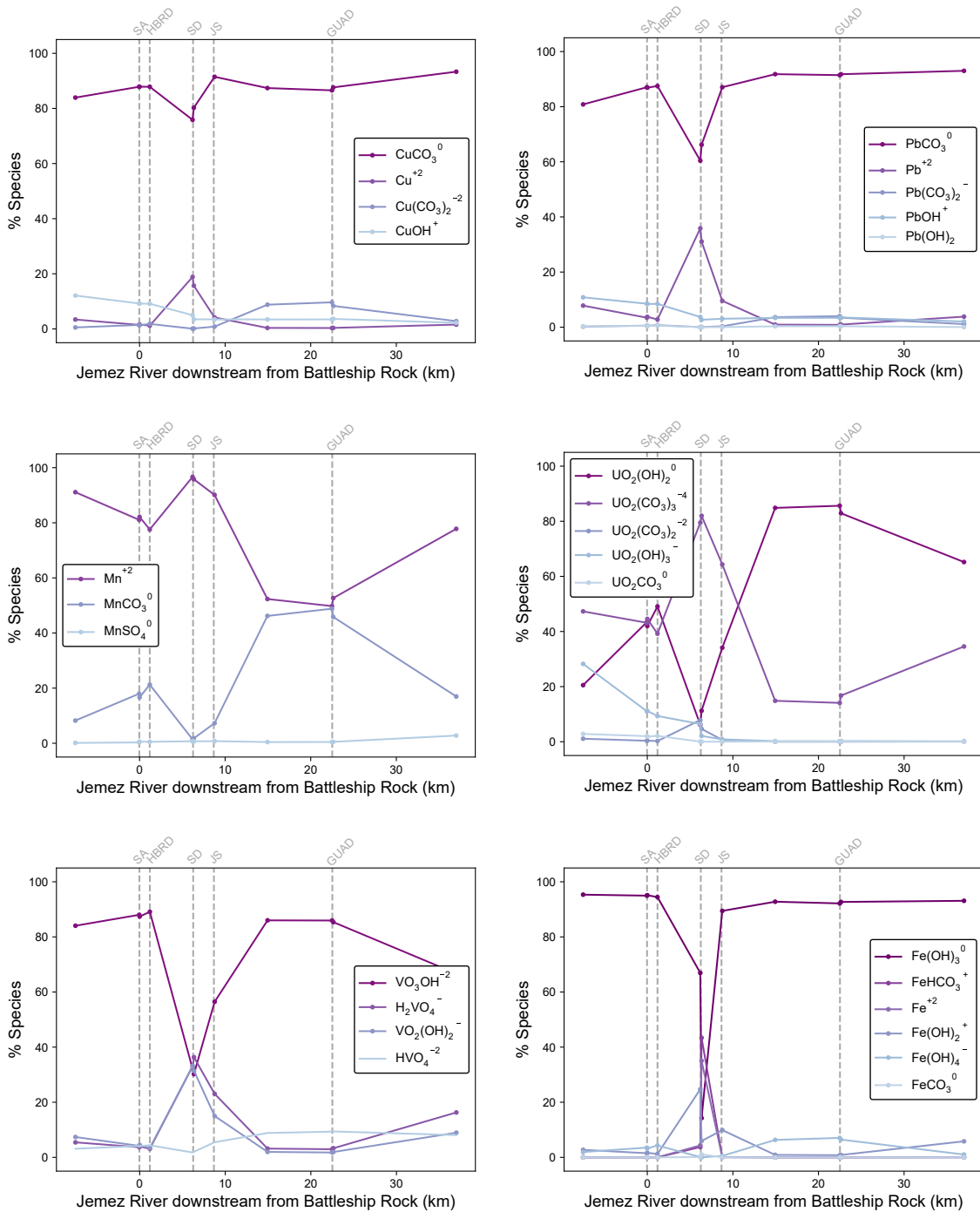


Figure 8 (cont.): Results of inorganic speciation modeling with Phreeqc. Any species contributing to $\leq 0.01\%$ are not included.

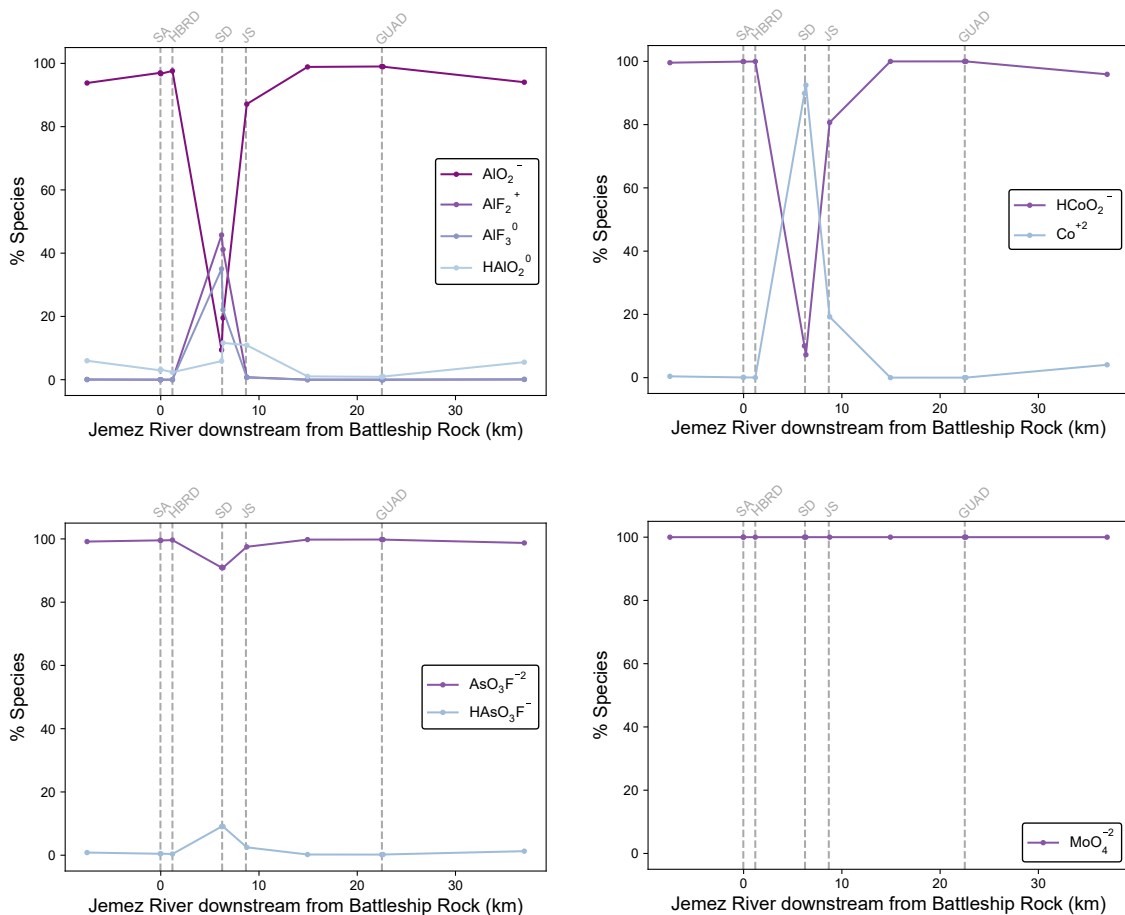


Figure 8 (cont.): Results of inorganic speciation modeling with Phreeqc. Any species contributing to $\leq 0.01\%$ are not included.

2002). Perhaps an even more important factor to consider is the transport of particular metals (Fe, U, Cu, Pb) that are known to become more readily adsorbed as neutral aqueous complexes (Figure 3), precluding any influence from charged solid surfaces. These unique in-situ geochemical conditions elicit preservation of the dissolved load of these transition metals.

The behavior of elements along the terminal part of the JR study reach is dependent on the inflowing end-member groundwaters (Figure 7). The significant increase in Sr and Ba concentrations is a result of interaction between the end-member fluids and marine sediments, as observed with the representative well waters (Figure 5). Unlike the highly soluble Li, Rb and Cs tend to become incorporated into feldspars, clays, and zeolites (Berger et al.,

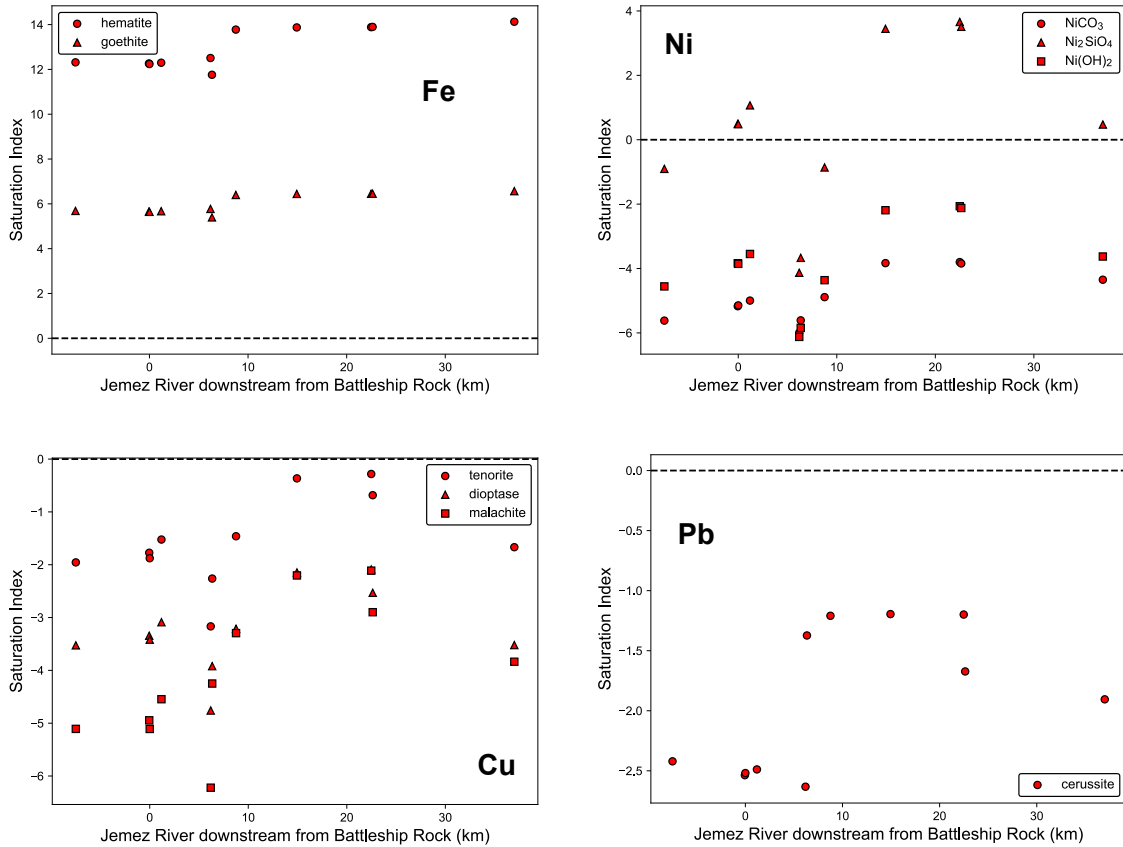


Figure 9: Saturation index of Jemez River waters with respect to Fe, Ni, U, Cu, Pb, Al, and Mn phases. The dashed line (Saturation Index = 0) denotes equilibrium.

1988; Ellis and Mahon, 1967), and are, thus, likely progressively becoming depleted in the end-member water as it travels along the flow path to mix with the JR. The addition of Fe, U, and Ni correspond with elevated signatures in the JP-1 and GT-01 wells. No well data are available to directly explain the increase in V, but the element often mimics the behavior of U (Railsback, 2003), especially in sedimentary settings (Hostetler and Garrels, 1962). Although Cu and Pb are enriched in the JP-1 well, these solutes are probably relatively absent in the actual end-member fluids mixing with the JR in San Ysidro.

3.3 Non-conservative trace elements

Trace elements that show unique non-conservative behavior (elsewhere besides HBRD) and/or appear to be depleted in the inflowing thermal waters are discussed individually

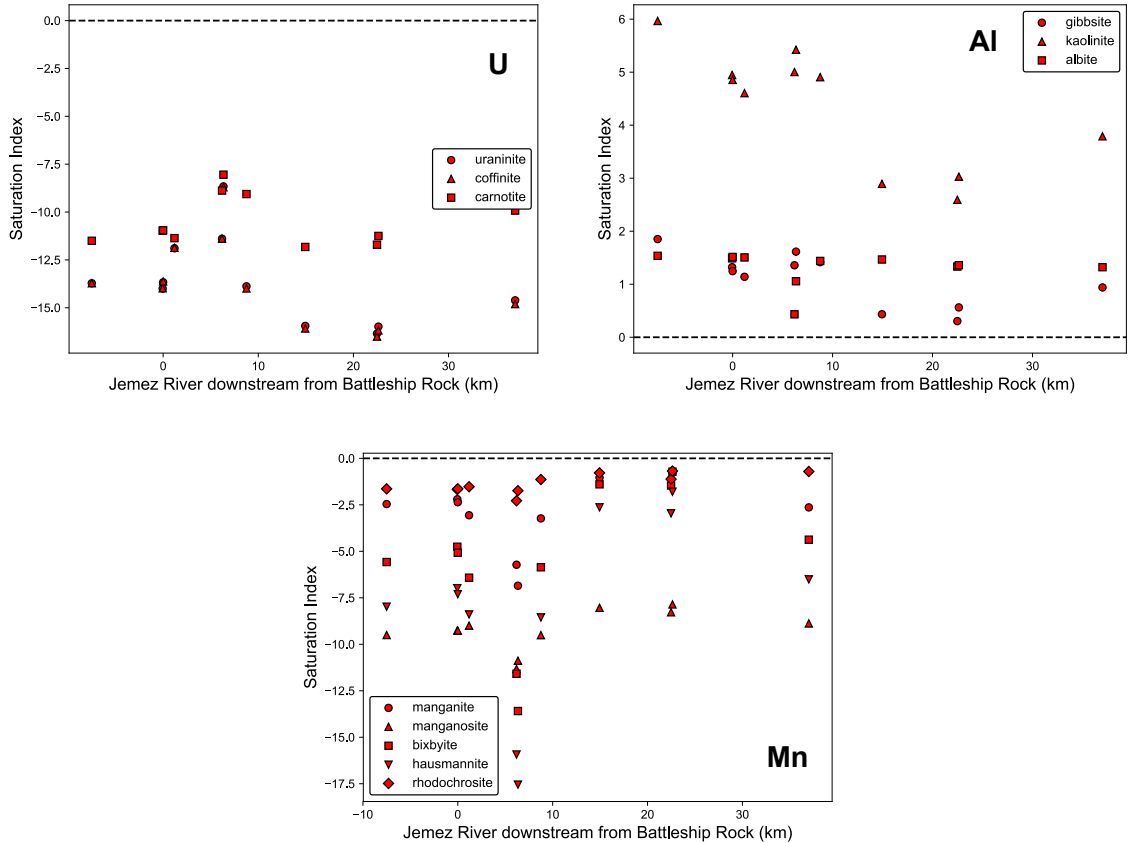


Figure 9 (cont.): Saturation index of Jemez River waters with respect to Fe, Ni, U, Cu, Pb, Al, and Mn phases. The dashed line (Saturation Index = 0) denotes equilibrium.

below.

3.3.1 Arsenic

Elevated concentrations of As in geothermal fluids and surface discharges have been associated with volcanogenic geothermal systems (Stauffer and Thompson, 1984; Webster and Nordstrom, 2003), with anomalously high levels of ≤ 48 ppm reported in the El Tatio geothermal field, Chile (Ellis and Mahon, 1977). Within the study reach, the highest measured values are found at SD ($174 \mu\text{M}$) and JS ($51 \mu\text{M}$) thermal springs (Figure 10). Correspondingly, there is as much of an 11.5-fold increase in As from the JR above to below the SD input. Exclusive non-conservative behavior of As is marked by the river section between this area of greatest loading and the town of Jemez Springs. The concentration of

As is expected to increase slightly or remain relatively constant since the JS inflow is more enriched relative to the last JR point. Instead, about 60% of introduced As at SD is removed from solution.

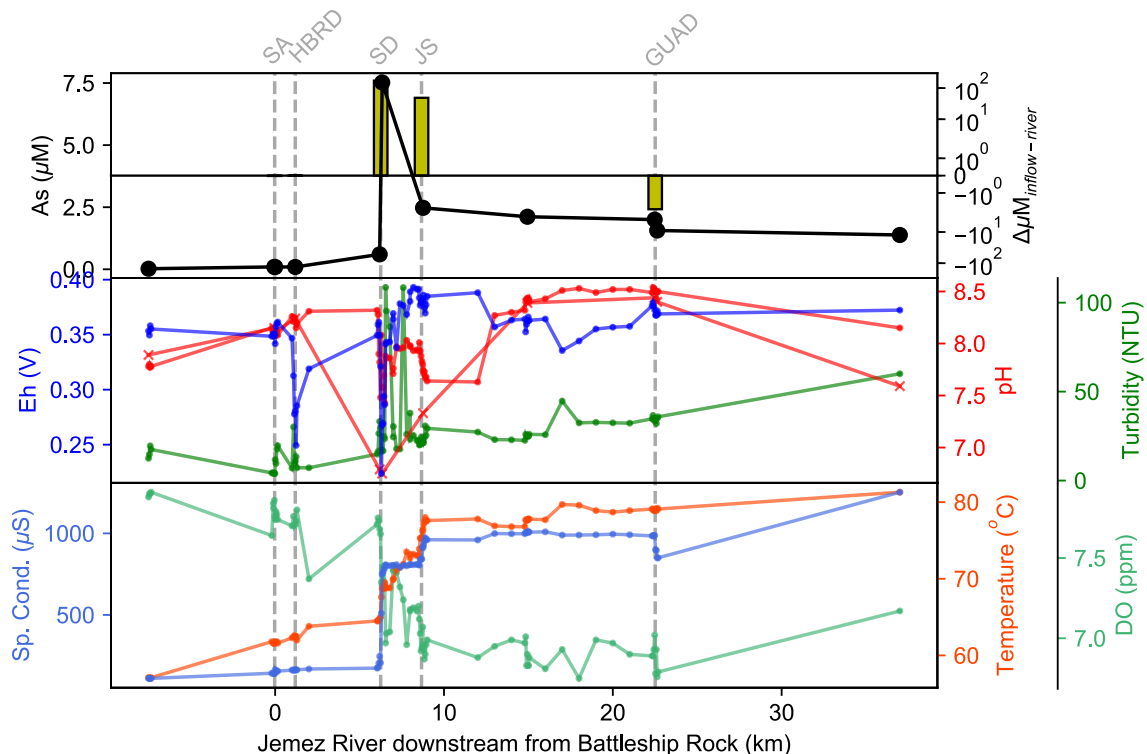


Figure 10: Subplots of arsenic downstream profile and spatial surveys of physiochemical parameters. The term, $\Delta\mu\text{M}_{\text{inflow-river}}$, is the difference in concentration between a known inflow and the preceding river sample. The line connected with ‘x’ markers denotes $\text{pH}_{\text{Oakton}}$.

Although As may stably exist in the environment in four oxidation states (+5, +3, 0, or -3), arsenite (+3) and arsenate (+5) are most common in aqueous systems. Due to the reducing and/or anaerobic conditions, arsenite has been noted to be the dominant form of As issuing from thermal springs (Bundschuh and Maity, 2015; Smedley and Kinniburgh, 2002; Webster and Nordstrom, 2003). Criaud and Fouillac (1989) report 57% of total As in SD emerges as arsenite. During an August 2015 campaign (~934 L/s), more recent work by Hansson (2016) determined that 55-72% of total As is arsenite at multiple SD seeps while 76% is present as arsenate at a JR point just below thermal inflow. The coexistence of both species may reflect the limitations reduced sulfur species impose on microbial and inorganic

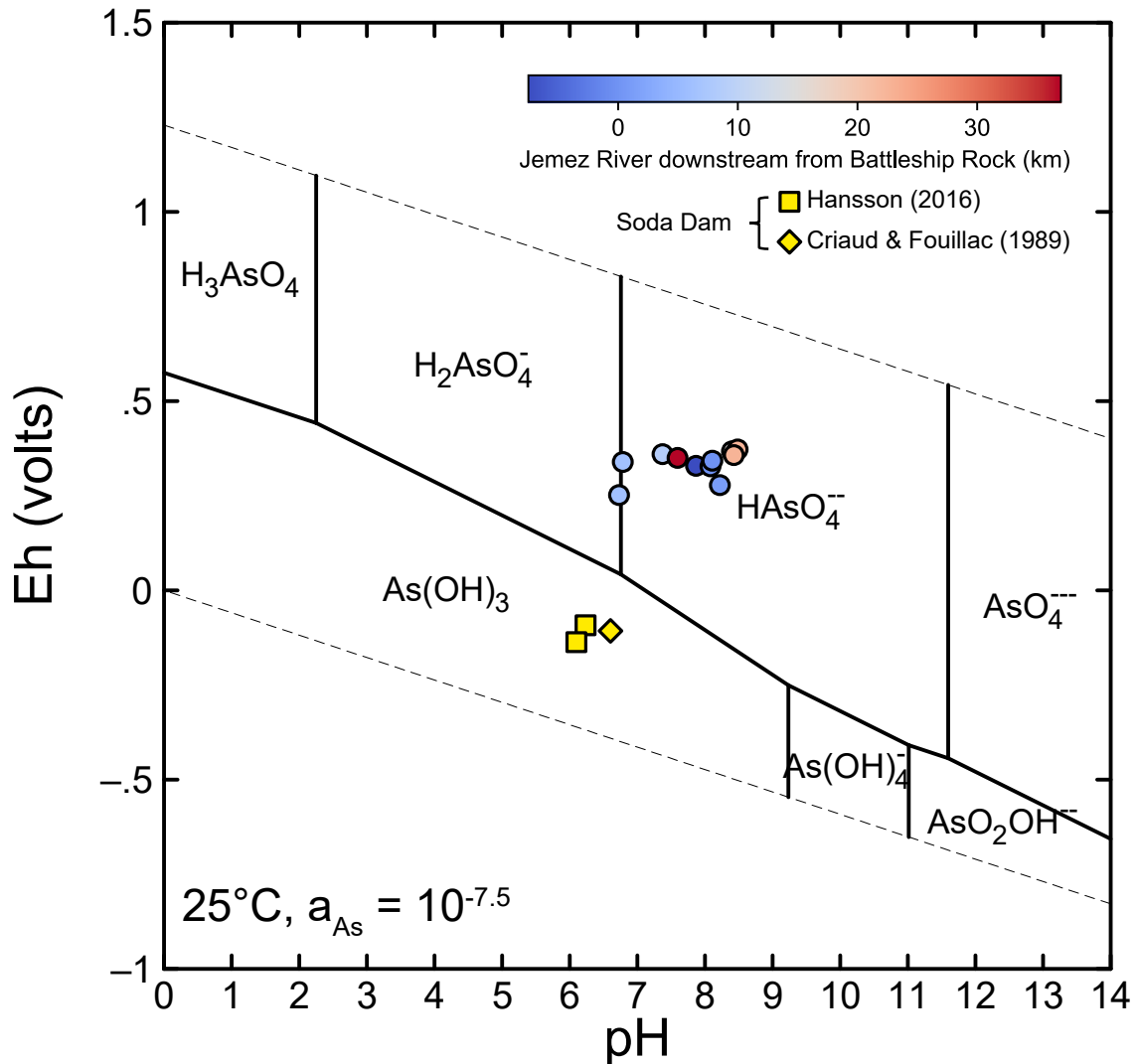


Figure 11: A Pourbaix (Eh-pH) diagram for aqueous arsenic species with Jemez River waters plotted.

As oxidation (Cherry et al., 1979; D’Imperio et al., 2007; Stauffer et al., 1980). Although there are significant changes to Eh-pH conditions, reaching respective global minima of 0.22 V and 7.43 pH_{YSI} (Fig. 9), just after the SD inflow, previous studies and a theoretical assessment (Figure 11) support likely predominance of arsenate, which could be controlling the fate of newly introduced As in-stream.

Along the JR section where As is behaving non-conservatively, there are sharp increases in turbidity, in addition to aforementioned decreases in Eh and pH (Figure 10). The most prominent increases occur just 0.3 km after the SD inflow (108.6 NTU) and approximately

at the midpoint (at 7.6 km) of SD and JS (108.5 NTU). This degradation in water transparency may support elevated presence of particulate matter, some of which may act as potential adsorbents. Relative to arsenite, it has been empirically demonstrated that arsenate has a higher potential to adsorb onto solids. The kinetics of arsenate adsorption are faster, and adsorption onto Fe, Al, and Mn oxides/oxyhydroxides is the most efficient at a pH range of 4-8 (Gupta and Chen, 1978; Raven et al., 1998), which are conditions reflected by the SD-mixed JR section where there is non-conservative transport of As.

3.3.2 Molybdenum

Unlike other conservative trace metals (subsection 3.2), the first and most significant increase in Mo concentration is at the confluence with SA (Figure 12), which is likely receiving some input from Mo-rich SPNC spring (Figure 5). There is no net positive contribution of Mo from the thermal springs, as their measured concentrations only make up 3.4-4.3% of those for the respective river points before inflow. Mo in geothermal fluids are not usually found in high concentrations, except for basalt-hosted systems (Arnórsson and Ívarsson, 1985; Evans et al., 2015; Kaasalainen and Stefánsson, 2012) that report as much as 0.73 μM (Arnórsson and Ívarsson, 1985). Furthermore, the range of Mo ($1.7\text{-}6.7 \times 10^{-2} \mu\text{M}$) found in the JR is comparable to an estimated background range worldwide ($1.1\text{-}8.9 \times 10^{-2} \mu\text{M}$) (Linnik and Ignatenko, 2015).

For the most part, the downstream profile of Mo is conservative. The majority of fluxes in concentration is attributed to mixing. Non-conservative behavior is identified at HBRD, where 0.01 μM is removed from solution, which may be explained by a local 60 NTU maximum (Figure 12). Although peak adsorption of Mo onto metal oxides, clays, and soils occurs around pH 3-5 (Goldberg et al., 1996; Matern and Mansfeldt, 2015), the alkaline conditions at HBRD do not preclude complete adsorption inactivity at pH slightly above circumneutral. The slight loss in Mo concentrations at HBRD may be attributed to weaker adsorption at high pH. However, this suggested mechanism does not appear to occur in

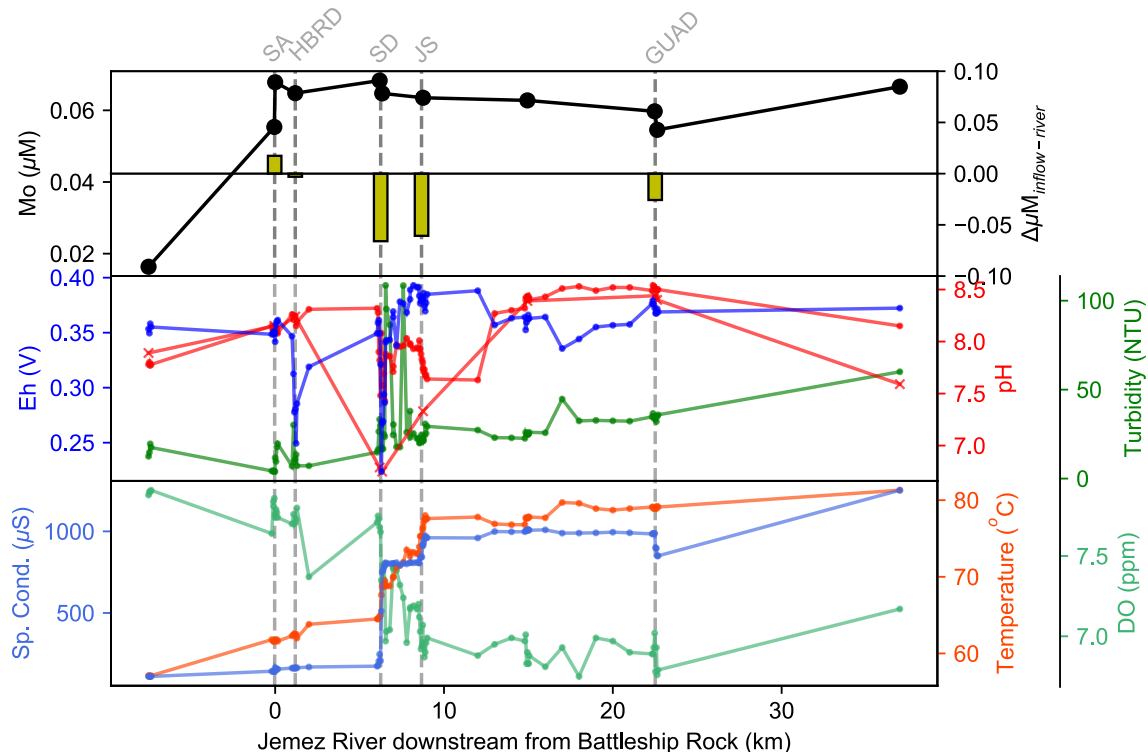


Figure 12: Subplots of molybdenum downstream profile and spatial surveys of physiochemical parameters. The term, $\Delta\mu\text{M}_{\text{inflow-river}}$, is the difference in concentration between a known inflow and the preceding river sample. The line connected with 'x' markers denotes $\text{pH}_{\text{Oakton}}$.

another JR section where physiochemical conditions would seem to favor stronger adsorption. Despite observing the lowest pH and highest turbidity along the stretch between SD and JS, there is less decrease in concentration between these two sampling points relative to HBRD (Figure 12). Hence, this disparity suggests that non-conservative behavior of Mo is not from adsorption.

The exclusive removal of Mo at HBRD may be governed by geochemical behavior analogous to a process responsible for creating enriched Mo deposits during euxinic events (Arnold et al., 2004; Neubert et al., 2008). Mo in the oxygenated JR waters likely exists predominantly as molybdate (MoO_4^{2-}), which is a highly soluble aqueous species. The JR waters at HRBD are within the range of seawater pH (7.5-8.4), where the oxygen in MoO_4^{2-} is susceptible to becoming replaced by larger, polarizable atoms from soft Lewis bases (Felten et al., 1978), such as S from incoming and dissolving H_2S , whose presence is maintained

by reducing conditions (Figure 12) and absence of ferrous iron (Figure 8; Stumm and Morgan, 1981). As a result, the dissolved Mo is progressively converted to some thiomolybdate species ($\text{MoO}_n\text{S}_{4-n}^{2-}$) (Erickson and Helz, 2000), which are more prone to removal via potential co-precipitation with Fe (Bertine, 1972; Helz et al., 2011), or other abundant transition metals. Dissolved Mo is more likely lost through sulfidation, transforming Mo into a reactive species, and eventual equilibrium coprecipitation. It is difficult to model any potential redox transitions due to the lack of reliable thermodynamic data for aqueous Mo species.

3.3.3 Aluminum

A significant control of aqueous Al activity is pH (Driscoll and Schecher, 1990; Hem and Roberson, 1967). Under acidic conditions, Al is soluble and exists mainly as the free Al^{3+} ion. Under circumneutral pH, Al is readily hydrolyzed into some aluminum hydroxyl group, which is relatively insoluble in water. The mean Al concentration for the JR, $0.68 \mu\text{M}$, which is well below estimated median concentration in North American rivers ($9 \mu\text{M}$; Durum and Haffty, 1963) and average concentration for freshwaters ($9 \mu\text{M}$; Bowen, 1966). Al is also generally scarce in neutral NaCl thermal waters, such as the SD ($0.91 \mu\text{M}$) and JS ($0.74 \mu\text{M}$) springs, but has been measured in 10^2 -ppm levels in acid- SO_4 condensates derived from geothermal steam or vapor systems (Goff et al., 1985; Lewis et al., 1997). Since podzolization (Cronan and Schofield, 1979; Lundström et al., 2000; Mokma and Burman, 1982) is unlikely to occur in a semi-arid watershed, the elevated Al signatures at East Fork JR and below GUAD (Figure 13) may be associated to the boggy conditions at those junctions. The East Fork headwater catchment has been observed to yield elevated concentrations of dissolved organic carbon (Chorover et al., 2011; McIntosh et al., 2016; Vázquez-Ortega et al., 2015), which can act as solubilizing agents of heavy metals such as Al (Sposito, 2008; Trostle et al., 2016). Moreover, further Al input to East Fork JR is likely coming from MCLY spring ($6.1 \mu\text{M}$; Figure 5).

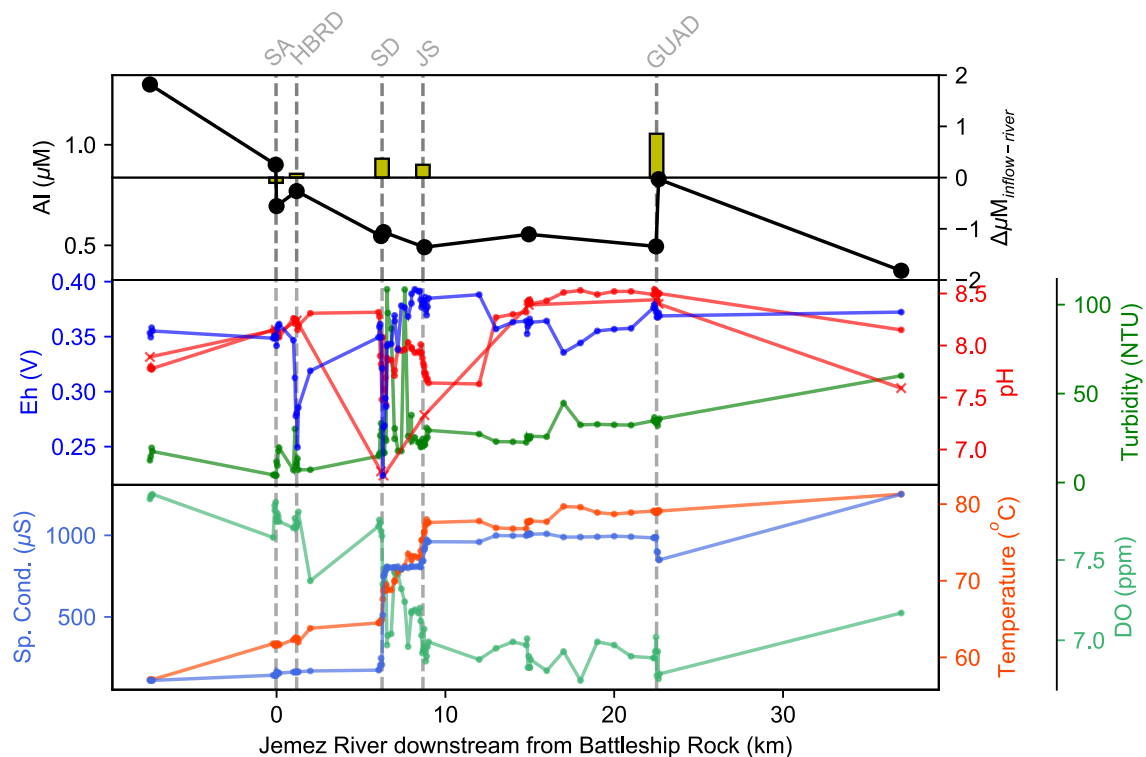


Figure 13: Subplots of aluminum downstream profile and spatial surveys of physiochemical parameters. The term, $\Delta\mu\text{M}_{\text{inflow-river}}$, is the difference in concentration between a known inflow and the preceding river sample. The line connected with 'x' markers denotes $\text{pH}_{\text{Oakton}}$.

For most of the river reach, the dissolved Al load is attenuated (Figure 13). It is possible that there is Al uptake from potentially precipitating gibbsite, kaolinite, or albite, as these phases appear to be supersaturated through all of the river reach (Figure 9). Some Al may also be lost to adsorption onto clay particulates (Charlet et al., 1993; Walker et al., 1988). This phenomenon is most clearly observed at the JR section between the two thermal spring inputs where there is loss of Al, even though the inflowing JS waters are more Al-loaded. There is a slight increase ($\sim 0.07 \mu\text{M}$ or $\sim 2 \mu\text{g/L}$) at HBRD, which is potentially receiving loading of Al via acidic solubilization (Driscoll, 1985; Driscoll and Schecher, 1990). Copious hydrothermal gas input charges soil solution, or water stored in streambed, with CO_2 , which dissolves into H_2CO_3 . The dissociation of H_2CO_3 increases concentration of H^+ , which releases particulate Al into solution, and produces HCO_3^- , which may act as a mobilizing counterion to Al. The 0.18 increase in pH from the Battleship confluence to

HBRD may mark infiltration of the high-pCO₂ Al-rich solution, as H⁺ is consumed during release of CO₂ from the dissolved inorganic carbon pool (no addition of HCO₃ at HBRD from JR at Battleship; Figure 6) upon exposure to atmospheric conditions.

3.3.4 Manganese

The occurrence of Mn in natural waters has been linked to plant metabolism, as the metal has been found to have been stored in tree leaves as a result of organic circulation (Bidwell et al., 2002; Ovington, 1956). Mn is also an abundant element in igneous ore minerals (Borchert, 1970), so its presence in the JR could be attributed to weathering of soil sourced from local volcanic material. With such a relatively short time-scale under the context of mass

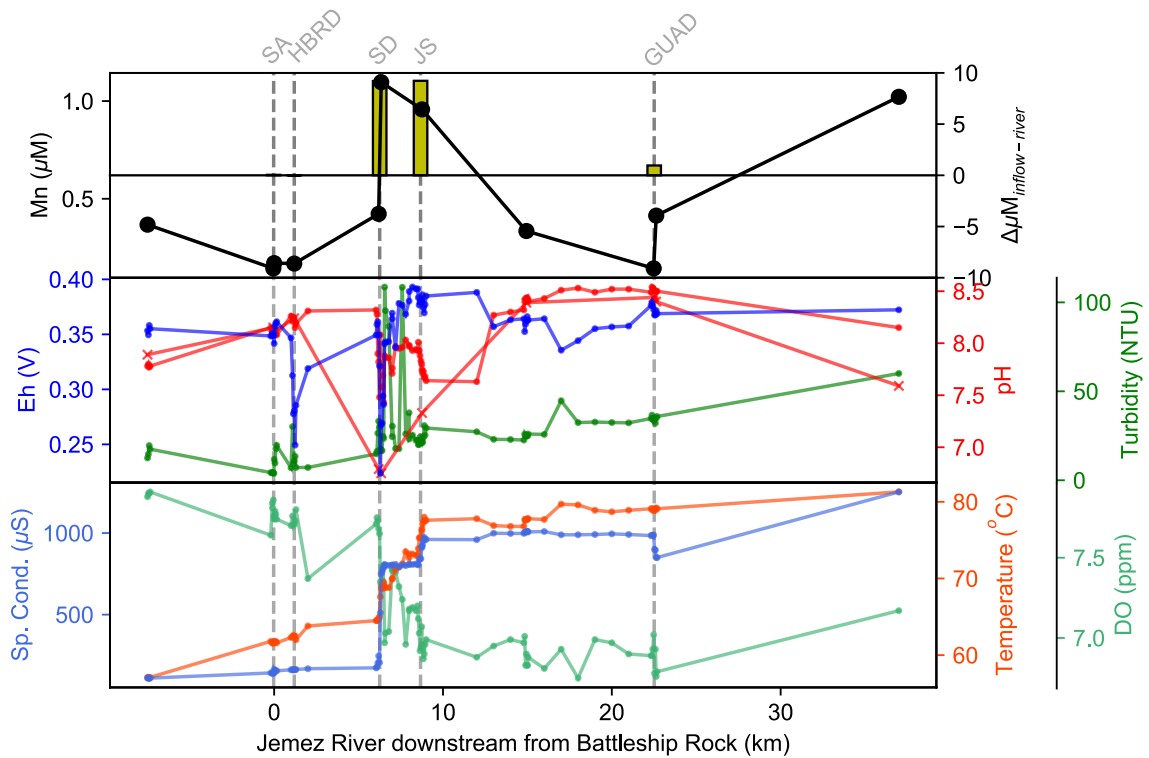


Figure 14: Subplots of manganese downstream profile and spatial surveys of physiochemical parameters. The term, $\Delta\mu\text{M}_{\text{inflow-river}}$, is the difference in concentration between a known inflow and the preceding river sample. The line connected with 'x' markers denotes pH_{Oakton}.

transport in a river, the slow kinetics of oxidation of Mn (Hem and Roberson, 1967; Laxen et al., 1984) likely do not affect speciation. Inorganic speciation modeling suggests that Mn

exists predominantly as Mn^{2+} in river stretches where concentrations are increasing and as aqueous MnCO_3 where the solute is depleting (Figures 8 and 14). Although Chiswell and Mokhtar (1986) state that $\text{MnCO}_{3(\text{aq})}$ is an insoluble form of Mn(II), the JR is undersaturated with respect to rhodochrosite and other solid phases (Figure 9). Some removal may also be mediated by adsorption to particulate matter, since the JR becomes progressively more turbid downstream.

4 Summary & Conclusions

We investigated natural salinization of the Jemez River during a low-flow event, as downstream aqueous geochemistry is influenced by its two tributaries and multiple areas of geothermal activity. There is a net ~ 500 -ppm increase from above the thermal springs to the end of the study reach. Major-solute behavior has been extensively characterized and has been identified to be governed by conservative processes through mixing. The abundance and distribution of accompanying trace elements, some of which have never been measured for the Jemez River before, appear to be dependent on changing hydrogeochemical compositions and unique in-situ physiochemical conditions along the study reach.

Two-thirds of measured trace elements mimic most of major-solute behavior. Relative non-reactivity of this group is characterized by weak ionic potential, constant oxidation state, and counterion balancing through complexation. To some extent, the presence of silica in these waters may potentially inhibit effective adsorption, which would allow these elements to remain in solution after receiving greatest loading from the Soda Dam thermal inflow. Conversely, the latter one-third is attenuated non-conservatively at different Jemez River sections by distinctive sinks attributed to adsorption, co-precipitation, and oxidation-enhanced immobility. Notably, some elements from both groups appear to be influenced at Hummingbird, where no aqueous inflows exist. There are considerable changes in Cu, Pb, and U concentrations, which could be attributed to the sudden shift to a more reducing system. More complex dynamics are likely responsible for fluctuations in Al and Mo at Hummingbird, where the Eh-pH state couples with upwelling hydrothermal gases to create environmental conditions commonly reserved to acidic environments and euxinic basins, respectively.

With persistent droughts and diminishing snowpack, properly managing water resources becomes even more imperative, especially in semi-arid regions like the southwestern U.S. This work emphasizes the importance of interactions between groundwater and surface wa-

ter, with implications for improving predictive models of water quality and refining general understanding of salinization dynamics.

References

- Albrecht, M., Kelley, S. A., Goff, F., Gardner, J. N., WoldeGabriel, G., and Welch, V. (2015). Innovative Exploration Techniques for Geothermal Assessment at Jemez Pueblo, New Mexico. Final Report DOE DE-EE0002841.
- Arnold, G. L., Anbar, A. D., Barling, J., and Lyons, T. W. (2004). Molybdenum Isotope Evidence for Widespread Anoxia in Mid-Proterozoic Oceans. *Science*, 304(5667):87–90.
- Arnórsson, S. and Ívarsson, G. (1985). Molybdenum in Icelandic geothermal waters. *Contributions to Mineralogy and Petrology*, 90(2):179–189.
- Association, A. P. H., Association, A. W. W., and Federation, W. E. (2018). 2320 alkalinity (2017). In *Standard Methods For the Examination of Water and Wastewater*, Standard Methods for the Examination of Water and Wastewater. American Public Health Association.
- Bau, M. (1991). Rare-earth element mobility during hydrothermal and metamorphic fluid-rock interaction and the significance of the oxidation state of europium. *Chemical Geology*, 93(3):219–230.
- Berger, G., Schott, J., and Guy, C. (1988). Behavior of Li, Rb and Cs during basalt glass and olivine dissolution and chlorite, smectite and zeolite precipitation from seawater: Experimental investigations and modelization between 50° and 300°C. *Chemical Geology*, 71(4):297–312.
- Bertine, K. K. (1972). The deposition of molybdenum in anoxic waters. *Marine Chemistry*, 1(1):43–53.
- Bidwell, S. D., Woodrow, I. E., Batianoff, G. N., and Sommer-Knudsen, J. (2002). Hyperaccumulation of manganese in the rainforest tree *Austromyrtus bidwillii* (Myrtaceae) from Queensland, Australia. *Functional Plant Biology*, 29(7):899–905.

- Borchert, H. (1970). On the ore-deposition and geochemistry of manganese. *Mineralium Deposita*, 5(3):300–314.
- Bowen, H. J. M. (1966). *Trace elements in biochemistry*. London, New York: Academic Press.
- Brookins, D. G. (1988). *Eh-pH Diagrams for Geochemistry*. Springer-Verlag, Berlin Heidelberg.
- Bundschuh, J. and Maity, J. P. (2015). Geothermal arsenic: Occurrence, mobility and environmental implications. *Renewable and Sustainable Energy Reviews*, 42:1214–1222.
- Charlet, L., Schindler, P. W., Spadini, L., Furrer, G., and Zysset, M. (1993). Cation adsorption on oxides and clays: The aluminum case. *Aquatic Sciences*, 55(4):291–303.
- Cherry, J. A., Shaikh, A. U., Tallman, D. E., and Nicholson, R. V. (1979). Arsenic Species as an Indicator of Redox Conditions in Groundwater. In Back, W. and Stephenson, D. A., editors, *Developments in Water Science*, volume 12 of *Contemporary Hydrogeology*, pages 373–392. Elsevier.
- Chiswell, B. and Mokhtar, M. B. (1986). The speciation of manganese in freshwaters. *Talanta*, 33(8):669–677.
- Chorover, J., Troch, P. A., Rasmussen, C., Brooks, P. D., Pelletier, J. D., Breshears, D. D., Huxman, T. E., Kurc, S. A., Lohse, K. A., McIntosh, J. C., Meixner, T., Schaap, M. G., Litvak, M. E., Perdrial, J., Harpold, A., and Durcik, M. (2011). How Water, Carbon, and Energy Drive Critical Zone Evolution: The Jemez–Santa Catalina Critical Zone Observatory. *Vadose Zone Journal*, 10(3):884–899.
- Connell, S. D. (2011). Preliminary Study of the Geologic Framework of the Colorado Plateau: Middle Rio Grande Basin Transition, New Mexico. Open-File Report 539, New Mexico Bureau of Geology and Mineral Resource.

- Criaud, A. and Fouillac, C. (1989). The distribution of arsenic (III) and arsenic (V) in geothermal waters: Examples from the Massif Central of France, the Island of Dominica in the Leeward Islands of the Caribbean, the Valles Caldera of New Mexico, U.S.A., and southwest Bulgaria. *Chemical Geology*, 76(3):259–269.
- Cronan, C. S. and Schofield, C. L. (1979). Aluminum Leaching Response to Acid Precipitation: Effects on High-Elevation Watersheds in the Northeast. *Science*, 204(4390):304–306.
- Crossey, L. J., Fischer, T. P., Patchett, P. J., Karlstrom, K. E., Hilton, D. R., Newell, D. L., Huntoon, P., Reynolds, A. C., and Leeuw, G. A. M. d. (2006). Dissected hydrologic system at the Grand Canyon: Interaction between deeply derived fluids and plateau aquifer waters in modern springs and travertine. *Geology*, 34(1):25–28.
- Crossey, L. J., Karlstrom, K. E., Dorsey, R., Pearce, J., Wan, E., Beard, L. S., Asmerom, Y., Polyak, V., Crow, R. S., Cohen, A., Bright, J., and Pecha, M. E. (2015). Importance of groundwater in propagating downward integration of the 6–5 Ma Colorado River system: Geochemistry of springs, travertines, and lacustrine carbonates of the Grand Canyon region over the past 12 Ma. *Geosphere*, 11(3):660–682.
- Crossey, L. J., Karlstrom, K. E., Springer, A. E., Newell, D., Hilton, D. R., and Fischer, T. (2009). Degassing of mantle-derived CO₂ and He from springs in the southern Colorado Plateau region: Neotectonic connections and implications for groundwater systemsMantle volatiles in travertine springs. *GSA Bulletin*, 121(7-8):1034–1053.
- Crossey, L. J., Sherson, L. S., Karlstrom, K. E., McGibbon, C., Jochems, A. P., Ali, A. M. S., Person, M., Dahm, C. N., and Parmenter, R. R. (2013). The water quality challenge: Using new technology to track tectonic salinity contributions that impair surface and groundwater. In *2013 GSA Annual Meeting in Denver*. Geological Society of America.

- Davis, C. C., Chen, H.-W., and Edwards, M. (2002). Modeling Silica Sorption to Iron Hydroxide. *Environmental Science & Technology*, 36(4):582–587.
- Davranche, M. and Bollinger, J.-C. (2000). Heavy Metals Desorption from Synthesized and Natural Iron and Manganese Oxyhydroxides: Effect of Reductive Conditions. *Journal of Colloid and Interface Science*, 227(2):531–539.
- Dickson, A. G. (1981). An exact definition of total alkalinity and a procedure for the estimation of alkalinity and total inorganic carbon from titration data. *Deep Sea Research Part A. Oceanographic Research Papers*, 28(6):609–623.
- D’Imperio, S., Lehr, C. R., Breary, M., and McDermott, T. R. (2007). Autecology of an Arsenite Chemolithotroph: Sulfide Constraints on Function and Distribution in a Geothermal Spring. *Appl. Environ. Microbiol.*, 73(21):7067–7074.
- Dondanville, R. F. (1971). The hydrothermal geology of the Valles Caldera, Jemez Mountains, New Mexico. Open File Consultant Report 36, Union Oil Company of California.
- Driscoll, C. T. (1985). Aluminum in acidic surface waters: chemistry, transport, and effects. *Environmental Health Perspectives*, 63:93–104.
- Driscoll, C. T. and Schecher, W. D. (1990). The chemistry of aluminum in the environment. *Environmental Geochemistry and Health*, 12(1):28–49.
- Durum, W. H. and Haffty, J. (1963). Implications of the minor element content of some major streams of the world. *Geochimica et Cosmochimica Acta*, 27(1):1–11.
- Dyer, J. R. (2007). Groundwater-Surface Water Interactions: Effects of Geothermal Spring Inputs to Jemez River Water Quality. Master’s Thesis, University of New Mexico.
- Ellis, A. J. and Mahon, W. (1977). *Chemistry and geothermal systems*. Academic Press, New York.

- Ellis, A. J. and Mahon, W. A. J. (1967). Natural hydrothermal systems and experimental hot water/rock interactions (Part II). *Geochimica et Cosmochimica Acta*, 31(4):519–538.
- Elston, W. E. (1967). Summary of the mineral resources of Bernalillo, Sandoval, and Santa Fe Counties, New Mexico (exclusive of oil and gas). Bulletin 81, New Mexico Bureau of Mines and Mineral Resources.
- Erickson, B. E. and Helz, G. R. (2000). Molybdenum(VI) speciation in sulfidic waters:: Stability and lability of thiomolybdates. *Geochimica et Cosmochimica Acta*, 64(7):1149–1158.
- Evans, W., Bergfeld, D., Sutton, A., Lee, R., and Lorenson, T. (2015). Groundwater chemistry in the vicinity of the Puna Geothermal Venture Power Plant, Hawai‘i, after two decades of production. USGS Numbered Series 2015-5139, U.S. Geological Survey, Reston, VA. IP-068405.
- Felten, H. v., Wernli, B., Gamsjäger, H., and Baertschi, P. (1978). Oxygen exchange between oxo-anions and water in basic media: molybdate(2-) and tungstate(2-). *Journal of the Chemical Society, Dalton Transactions*, 0(5):496–500.
- Fuller, C. C. and Davis, J. A. (1989). Influence of coupling of sorption and photosynthetic processes on trace element cycles in natural waters. *Nature*, 340(6228):52.
- Gaillardet, J., Viers, J., and Dupré, B. (2003). 5.09 - Trace Elements in River Waters. In Holland, H. D. and Turekian, K. K., editors, *Treatise on Geochemistry*, pages 225–272. Pergamon, Oxford.
- Gardner, J. N., Goff, F., Garcia, S., and Hagan, R. C. (1986). Stratigraphic relations and lithologic variations in the Jemez Volcanic Field, New Mexico. *Journal of Geophysical Research: Solid Earth*, 91(B2):1763–1778.

- Garrels, R. M. and Christ, C. L. (1965). *Solutions, minerals, and equilibria*. Harper's geoscience series. Harper & Row, New York.
- Gascoyne, M. (1992). Geochemistry of the actinides and their daughters. In *Uranium-series disequilibrium: applications to earth, marine, and environmental sciences*. Clarendon Press, United Kingdom, 2nd edition.
- Gibbs, R. J. (1973). Mechanisms of Trace Metal Transport in Rivers. *Science*, 180(4081):71–73.
- Godtfredsen, K. L. and Stone, A. T. (1994). Solubilization of Manganese Dioxide-Bound Copper by Naturally Occurring Organic Compounds. *Environmental Science & Technology*, 28(8):1450–1458.
- Goff, F. (2009). *Valles Caldera: a geologic history*. UNM Press.
- Goff, F., Gardner, J., Vidale, R., and Charles, R. (1985). Geochemistry and isotopes of fluids from sulphur springs, Valles Caldera, New Mexico. *Journal of Volcanology and Geothermal Research*, 23(3):273–297.
- Goff, F., Gardner, J. N., Reneau, S. L., Kelley, S. A., Kempter, K. A., and Lawrence, J. R. (2011). Geologic map of the Valles caldera, Jemez Mountains, New Mexico. *New Mexico Bureau of Geology & Mineral Resources*, 79.
- Goff, F. and Grigsby, C. O. (1982). Valles Caldera geothermal systems, New Mexico, U.S.A. *Journal of Hydrology*, 56(1):119–136.
- Goff, F., Grigsby, C. O., Trujillo, P. E., Counce, D., and Kron, A. (1981). Geology, water geochemistry and geothermal potential of the jemez springs area, Canon de San Diego, new Mexico. *Journal of Volcanology and Geothermal Research*, 10(1):227–244.
- Goff, F., Shevenell, L., Gardner, J. N., Vuataz, F.-D., and Grigsby, C. O. (1988). The hydrothermal outflow plume of Valles Caldera, New Mexico, and a comparison with

- other outflow plumes. *Journal of Geophysical Research: Solid Earth*, 93(B6):6041–6058.
- Goldberg, S., Forster, H. S., and Godfrey, C. L. (1996). Molybdenum Adsorption on Oxides, Clay Minerals, and Soils. *Soil Science Society of America Journal*, 60(2):425–432.
- Graf, D. L. (1962). Minor element distribution in sedimentary carbonate rocks. *Geochimica et Cosmochimica Acta*, 26(8):849–856.
- Gran, G. (1952). Determination of the equivalence point in potentiometric titrations. Part II. *Analyst*, 77(920):661–671.
- Gupta, S. K. and Chen, K. Y. (1978). Arsenic Removal by Adsorption. *Journal (Water Pollution Control Federation)*, 50(3):493–506.
- Hansson, L. (2016). *Concentrations and riverine massflows of geothermal arsenic. : Case study: Jemez River, NM, USA*. Student thesis, Stockholm University.
- Hedenquist, J. W. and Lowenstern, J. B. (1994). The role of magmas in the formation of hydrothermal ore deposits. *Nature*, 370(6490):519.
- Heier, K. S. and Adams, J. A. S. (1964). The geochemistry of the alkali metals. *Physics and Chemistry of the Earth*, 5:253–381.
- Helz, G. R., Bura-Nakić, E., Mikac, N., and Ciglencečki, I. (2011). New model for molybdenum behavior in euxinic waters. *Chemical Geology*, 284(3):323–332.
- Hem, J. D. and Roberson, C. E. (1967). Form and stability of aluminum hydroxide complexes in dilute solution. USGS Numbered Series 1827-A, U.S. G.P.O.,.
- Henley, R. W. and Ellis, A. J. (1983). Geothermal systems ancient and modern: a geochemical review. *Earth-Science Reviews*, 19(1):1–50.

- Hostetler, P. B. and Garrels, R. M. (1962). Transportation and precipitation of uranium and vanadium at low temperatures, with special reference to sandstone-type uranium deposits. *Economic Geology*, 57(2):137–167.
- Hulen, J. B., Nielson, D. L., Goff, F., Gardner, J. N., and Charles, R. W. (1987). Molybdenum mineralization in an active geothermal system, Valles caldera, New Mexico. *Geology*, 15(8):748–752.
- Izett, G. A. and Obradovich, J. D. (1994). $^{40}\text{Ar}/^{39}\text{Ar}$ age constraints for the Jaramillo Normal Subchron and the Matuyama-Brunhes geomagnetic boundary. *Journal of Geophysical Research: Solid Earth*, 99(B2):2925–2934.
- Jochems, A. P., Sherson, L. R., Crossey, L. J., and Karlstrom, K. E. (2010). Predictive Analysis of Geochemical Controls in an Alpine Stream. In *AGU Fall Meeting Abstracts*, volume 31, pages H31D–1041.
- Johnson, D. B. and Hallberg, K. B. (2005). Acid mine drainage remediation options: a review. *Science of The Total Environment*, 338(1):3–14.
- Johnson, J., Anderson, G., and Parkhurst, D. L. (2000). Database “thermo. com. V8. R6. 230,” Rev. 1-11. *Lawrence Livermore Natl. Lab., Livermore, California*.
- Kaasalainen, H. and Stefánsson, A. (2012). The chemistry of trace elements in surface geothermal waters and steam, Iceland. *Chemical Geology*, 330-331:60–85.
- Kelley, S. A., Kempter, K. A., Goff, F., Rampey, M., Osburn, R. G., and Ferguson, C. A. (2003). Geologic Map of the Jemez Springs Quadrangle, Sandoval County, New Mexico. Open-file Digital Geologic Map OF-GM 073, New Mexico Bureau of Geology and Mineral Resources.
- Kelley, S. A., McIntosh, W. C., Goff, F., Kempter, K. A., Wolff, J. A., Esser, R., Braschayko,

- S., Love, D., and Gardner, J. N. (2013). Spatial and temporal trends in pre-caldera Jemez Mountains volcanic and fault activity. *Geosphere*, 9(3):614–646.
- Kelley, S. A., Osburn, R. G., and Kempter, K. A. (2007). Geology of Cañon de San Diego, southwestern Jemez Mountains, north-central New Mexico. In *New Mexico Geological Society 58th Annual Fall Field Conference Guidebook*, Geology of the Jemez Region II, pages 169–181. New Mexico Geological Society.
- Kirk, M. F., Crossey, L. J., Takacs-Vesbach, C., Newell, D. L., and Bowman, R. S. (2009). Influence of upwelling saline groundwater on iron and manganese cycling in the Rio Grande floodplain aquifer. *Applied Geochemistry*, 24(3):426–437.
- Kirk, M. F., Holm, T. R., Park, J., Jin, Q., Sanford, R. A., Fouke, B. W., and Bethke, C. M. (2004). Bacterial sulfate reduction limits natural arsenic contamination in groundwater. *Geology*, 32(11):953–956.
- Laxen, D. P. H., Davison, W., and Woof, C. (1984). Manganese chemistry in rivers and streams. *Geochimica et Cosmochimica Acta*, 48(10):2107–2111.
- Lewis, A. J., Palmer, M. R., Sturchio, N. C., and Kemp, A. J. (1997). The rare earth element geochemistry of acid-sulphate and acid-sulphate-chloride geothermal systems from Yellowstone National Park, Wyoming, USA. *Geochimica et Cosmochimica Acta*, 61(4):695–706.
- Lin, Y.-P. and Valentine, R. L. (2008). The Release of Lead from the Reduction of Lead Oxide (PbO₂) by Natural Organic Matter. *Environmental Science & Technology*, 42(3):760–765.
- Linnik, P. N. and Ignatenko, I. I. (2015). Molybdenum in Natural Surface Waters: Content and Forms of Occurrence (a Review). *Hydrobiological Journal*, 51(4).

- Lundström, U. S., van Breemen, N., and Bain, D. (2000). The podzolization process. A review. *Geoderma*, 94(2):91–107.
- Mapanda, F., Mangwayana, E. N., Nyamangara, J., and Giller, K. E. (2005). The effect of long-term irrigation using wastewater on heavy metal contents of soils under vegetables in Harare, Zimbabwe. *Agriculture, Ecosystems & Environment*, 107(2):151–165.
- Matern, K. and Mansfeldt, T. (2015). Molybdate adsorption by birnessite. *Applied Clay Science*, 108:78–83.
- McGibbon, C., Crossey, L. J., Karlstrom, K. E., and Grulke, T. (2018). Carbonic springs as distal manifestations of geothermal systems, highlighting the importance of fault pathways and hydrochemical mixing: Example from the Jemez Mountains, New Mexico. *Applied Geochemistry*, 98:45–57.
- McIntosh, J. C., Schaumberg, C., Perdrial, J., Harpold, A., Vázquez-Ortega, A., Rasmussen, C., Vinson, D., Zapata-Rios, X., Brooks, P. D., Meixner, T., Pelletier, J., Derry, L., and Chorover, J. (2016). Geochemical evolution of the Critical Zone across variable time scales informs concentration-discharge relationships: Jemez River Basin Critical Zone Observatory. *Water Resources Research*, pages 4169–4196.
- McLemore, V. T. (1996). Mineral resources in the Jemez and Nacimiento Mountains, Rio Arriba, Sandoval, Santa Fe and Los Alamos Counties, New Mexico. In *New Mexico Geological Society 47th Annual Fall Field Conference Guidebook*, Jemez Mountains Region, pages 161–168. New Mexico Geological Society.
- Mohiuddin, K. M., Zakir, H. M., Otomo, K., Sharmin, S., and Shikazono, N. (2010). Geochemical distribution of trace metal pollutants in water and sediments of downstream of an urban river. *International Journal of Environmental Science & Technology*, 7(1):17–28.

- Mokma, D. L. and Buurman, P. (1982). *Podzols and podzolization in temperate regions*. International Soil Museum, Wageningen.
- Nesbitt, H. W., Markovics, G., and price, R. C. (1980). Chemical processes affecting alkalis and alkaline earths during continental weathering. *Geochimica et Cosmochimica Acta*, 44(11):1659–1666.
- Neubert, N., Nögler, T. F., and Böttcher, M. E. (2008). Sulfidity controls molybdenum isotope fractionation into euxinic sediments: Evidence from the modern Black Sea. *Geology*, 36(10):775–778.
- New Mexico Environment Department (2016). Total Maximum Daily Load for the Jemez River Watershed. Technical report.
- Newell, D. L., Crossey, L. J., Karlstrom, K. E., Fischer, T. P., and Hilton, D. R. (2005). Continental-scale links between the mantle and groundwater systems of the western United States: Evidence from travertine springs and regional He isotope data. *GSA Today*, 15(12):4.
- Nieto, J. M., Sarmiento, A. M., Olías, M., Canovas, C. R., Riba, I., Kalman, J., and Delvalls, T. A. (2007). Acid mine drainage pollution in the Tinto and Odiel rivers (Iberian Pyrite Belt, SW Spain) and bioavailability of the transported metals to the Huelva Estuary. *Environment International*, 33(4):445–455.
- Nordstrom, D. K. and Wilde, F. D. (2005). Reduction Oxidation Potential (Electrode Method). In *National Field Manual for the Collection of Water-Quality Data (TWRI Book 9)*, number 6.5 in A6. U.S. Geological Survey.
- Ovington, J. D. (1956). The composition of tree leaves. *Forestry: An International Journal of Forest Research*, 29(1):22–28.

- Parkhurst, D. L. and Appelo, C. (2013). Description of input and examples for PHREEQC version 3: a computer program for speciation, batch-reaction, one-dimensional transport, and inverse geochemical calculations. USGS Numbered Series 6-A43, U.S. Geological Survey, Reston, VA.
- Pfaff, J. D. (1993). Method 300.0 Determination of inorganic anions by ion chromatography. *US Environmental Protection Agency, Office of Research and Development, Environmental Monitoring Systems Laboratory*, 28.
- Phillips, E. H., Goff, F., Kyle, P. R., McIntosh, W. C., Dunbar, N. W., and Gardner, J. N. (2007). The $^{40}\text{Ar}/^{39}\text{Ar}$ age constraints on the duration of resurgence at the Valles caldera, New Mexico. *Journal of Geophysical Research: Solid Earth*, 112(B8).
- Purtymun, W. D., West, F. G., and Adams, W. H. (1974). Preliminary study of the quality of water in the drainage area of the Jemez River and Rio Guadalupe. Technical Report LA-5595-MS, Los Alamos Scientific Lab., N.Mex. (US).
- Railsback, L. B. (2003). An Earth scientist's periodic table of the elements and their ions. *Geology*, 31(9):737–740.
- Raven, K. P., Jain, A., and Loeppert, R. H. (1998). Arsenite and Arsenate Adsorption on Ferrihydrite: Kinetics, Equilibrium, and Adsorption Envelopes. *Environmental Science & Technology*, 32(3):344–349.
- Reid, K. D., Goff, F., and Counce, D. A. (2003). Arsenic concentration and mass flow rate in natural waters of the Valles Caldera and Jemez Mountains region, New Mexico. *New Mexico Geology*, 25(3):75–81.
- Rittle, K. A., Drever, J. I., and Colberg, P. J. S. (1995). Precipitation of arsenic during bacterial sulfate reduction. *Geomicrobiology Journal*, 13(1):1–11.

- Sherson, L. R., Crossey, L. J., Van Horn, D., Dahm, C. N., and Parmenter, R. R. (2009). Geothermal contributions to water chemistry in the Jemez River: Implications for water quality management in the Rio Grande, New Mexico. In *2009 Portland GSA Annual Meeting*. Geological Society of America.
- Shiller, A. M., Duan, S., Erp, P. v., and Bianchi, T. S. (2006). Photo-oxidation of dissolved organic matter in river water and its effect on trace element speciation. *Limnology and Oceanography*, 51(4):1716–1728.
- Smedley, P. L. and Kinniburgh, D. G. (2002). A review of the source, behaviour and distribution of arsenic in natural waters. *Applied Geochemistry*, 17(5):517–568.
- Smith, J. (2016). CO₂ Flux Along Faults of the Central Rio Grande Rift, New Mexico. Master's Thesis, University of New Mexico.
- Spell, T. L. and Harrison, T. M. (1993). 40Ar/39Ar Geochronology of Post-Valles Caldera Rhyolites, Jemez Volcanic Field, New Mexico. *Journal of Geophysical Research: Solid Earth*, 98(B5):8031–8051.
- Sposito, G. (2008). *The Chemistry of Soils*. Oxford University Press, USA. Google-Books-ID: XCJnDAAAQBAJ.
- Stauffer, R. E., Jenne, E. A., and Ball, J. (1980). Chemical studies of selected trace elements in hot-spring drainages of Yellowstone National Park. USGS Numbered Series 1044-F, U.S. Govt. Print. Off.,.
- Stauffer, R. E. and Thompson, J. M. (1984). Arsenic and antimony in geothermal waters of Yellowstone National Park, Wyoming, USA. *Geochimica et Cosmochimica Acta*, 48(12):2547–2561.
- Stiff, H. A. J. (1951). The Interpretation of Chemical Water Analysis by Means of Patterns. *Journal of Petroleum Technology*, 3(10):15–3.

- Stumm, W. and Morgan, J. J. (1981). *Aquatic chemistry: an introduction emphasizing chemical equilibria in natural waters*. John Wiley & Sons.
- Szynkiewicz, A., Goff, F., Faiia, A. M., and Vaniman, D. (2019a). Sulfur cycle in the Valles Caldera volcanic complex, New Mexico – Letter 2: Aqueous sulfate budget and implications for hydrological transport on early Mars. *Earth and Planetary Science Letters*, 506:552–562.
- Szynkiewicz, A., Goff, F., Vaniman, D., and Pribil, M. J. (2019b). Sulfur cycle in the Valles Caldera volcanic complex, New Mexico – Letter 1: Sulfate sources in aqueous system, and implications for S isotope record in Gale Crater on Mars. *Earth and Planetary Science Letters*, 506:540–551.
- Szynkiewicz, A., Johnson, A. P., and Pratt, L. M. (2012). Sulfur species and biosignatures in Sulphur Springs, Valles Caldera, New Mexico—Implications for Mars astrobiology. *Earth and Planetary Science Letters*, 321-322:1–13.
- Trainer, F. W. (1978). Geohydrologic data from the Jemez Mountains and vicinity, north-central New Mexico. USGS Numbered Series 77-131, U.S. Geological Survey, Water Resources Division,.
- Trainer, F. W., Rogers, R. J., and Sorey, M. (2000). Geothermal hydrology of Valles Caldera and the southwestern Jemez Mountains, New Mexico. USGS Numbered Series 2000-4067, U.S. Department of the Interior, U.S. Geological Survey ; Information Services [distributor],.
- Trostle, K. D., Runyon, J. R., Pohlmann, M. A., Redfield, S. E., Pelletier, J., McIntosh, J., and Chorover, J. (2016). Colloids and organic matter complexation control trace metal concentration-discharge relationships in Marshall Gulch stream waters. *Water Resources Research*, pages 7931–7944.

- USGS (2019). USGS Current Conditions for USGS 08324000 JEMEZ RIVER NEAR JEMEZ, NM.
- Vuataz, F. D. and Goff, F. (1986). Isotope geochemistry of thermal and nonthermal waters in the Valles Caldera, Jemez Mountains, Northern New Mexico. *Journal of Geophysical Research: Solid Earth*, 91(B2):1835–1853.
- Vázquez-Ortega, A., Perdrial, J., Harpold, A., Zapata-Ríos, X., Rasmussen, C., McIntosh, J., Schaap, M., Pelletier, J. D., Brooks, P. D., Amistadi, M. K., and Chorover, J. (2015). Rare earth elements as reactive tracers of biogeochemical weathering in forested rhyolitic terrain. *Chemical Geology*, 391:19–32.
- Walker, W. J., Cronan, C. S., and Patterson, H. H. (1988). A kinetic study of aluminum adsorption by aluminosilicate clay minerals. *Geochimica et Cosmochimica Acta*, 52(1):55–62.
- Webster, J. G. and Nordstrom, D. K. (2003). Geothermal Arsenic. In Welch, A. H. and Stollenwerk, K. G., editors, *Arsenic in Ground Water: Geochemistry and Occurrence*, pages 101–125. Springer US, Boston, MA.
- Wilde, F. D. (2006). Collection of Water Samples. In *National Field Manual for the Collection of Water-Quality Data (TWRI Book 9)*, A4. U.S. Geological Survey.
- Williams, A. J., Crossey, L. J., Karlstrom, K. E., Newell, D., Person, M., and Woolsey, E. (2013). Hydrogeochemistry of the Middle Rio Grande aquifer system — Fluid mixing and salinization of the Rio Grande due to fault inputs. *Chemical Geology*, 351:281–298.
- Zimmerer, M. J., Lafferty, J., and Coble, M. A. (2016). The eruptive and magmatic history of the youngest pulse of volcanism at the Valles caldera: Implications for successfully dating late Quaternary eruptions. *Journal of Volcanology and Geothermal Research*, 310:50–57.

Appendix A Field Photos



Field photographs of riverside geothermal features: bleached outcrops at Hummingbird site (A & B) and travertine deposits at Jemez Springs (C) and Soda Dam (D).

Appendix B Spatial Series Data

Spatial series data of physiochemical parameters over ~50-km Jemez River reach:

| Site | Sp. Cond. ($\mu\text{S}/\text{cm}$) | TDS (mg/L) | Temp. ($^{\circ}\text{C}$) | pH | ORP (mV) | Turbidity (NTU) | ODO (ppm) | Distance (km) |
|----------------|---------------------------------------|------------|------------------------------|------|----------|-----------------|-----------|---------------|
| JG01 (EFJRH4) | 111 | 72 | 13.94 | 7.78 | 143.3 | 12.53 | 7.88 | -7.5 |
| JG02 | 111 | 72 | 13.94 | 7.8 | 139.5 | 14.7 | 7.9 | -7.45 |
| JG03 | 111.1 | 72 | 13.89 | 7.77 | 148 | 19.5 | 7.9 | -7.4 |
| JG04 | 111 | 72 | 13.94 | 7.78 | 145.1 | 17.49 | 7.91 | -7.35 |
| JG13 | 142.7 | 93 | 16.56 | 8.15 | 141.1 | 4.31 | 7.64 | -0.2 |
| JG11 | 141.8 | 92 | 16.44 | 8.08 | 143.1 | 4.18 | 7.84 | -0.11 |
| JG10 (EFJRABR) | 141.8 | 92 | 16.44 | 8.11 | 141 | 4.26 | 7.81 | -0.1 |
| JG09 | 141.9 | 92 | 16.44 | 8.09 | 143.2 | 4.09 | 7.86 | -0.05 |
| JG12 | 141.9 | 92 | 16.50 | 8.09 | 141.9 | 3.93 | 7.76 | -0.015 |
| JG14 (JRBBR) | 164.8 | 107 | 16.44 | 8.12 | 134.2 | 11.73 | 7.74 | 0 |
| JG15 | 155.7 | 101 | 16.50 | 8.11 | 149.6 | 9.62 | 7.79 | 0.05 |
| JG16 | 155.5 | 101 | 16.56 | 8.12 | 152.7 | 17.71 | 7.77 | 0.1 |
| JG17 | 155.7 | 101 | 16.44 | 8.08 | 153.9 | 19.59 | 7.74 | 0.15 |
| JG18 | 162 | 105 | 16.83 | 8.26 | 139.6 | 7.01 | 7.7 | 1 |
| JG19 | 162.2 | 105 | 16.89 | 8.21 | 105.5 | 30.19 | 7.76 | 1.09 |
| JG20 | 162.2 | 105 | 17.00 | 8.25 | 70.8 | 9.53 | 7.7 | 1.14 |
| JG21 (HBRD) | 162.5 | 106 | 16.94 | 8.24 | 73.3 | 10.97 | 7.71 | 1.19 |
| JG22 | 162.4 | 106 | 16.94 | 8.15 | 42.3 | 13.44 | 7.73 | 1.24 |
| JG23 | 164 | 107 | 16.67 | 8.19 | 78.1 | 7.19 | 7.8 | 1.29 |
| JG24 | 168.7 | 110 | 17.67 | 8.31 | 112.6 | 7.18 | 7.37 | 2 |
| JG30 | 173.9 | 113 | 18.06 | 8.32 | 143.4 | 14.82 | 7.71 | 6.04 |
| JG31 | 177.9 | 116 | 18.06 | 8.28 | 153 | 16.24 | 7.75 | 6.09 |
| JG32 | 204.1 | 133 | 18.11 | 7.9 | 155.6 | 26.46 | 7.73 | 6.14 |
| JG33 (JRASD) | 247.1 | 161 | 18.22 | 7.82 | 143.6 | 33.25 | 7.68 | 6.19 |
| JG34 | 206.4 | 134 | 18.33 | 7.48 | 115.5 | 29.75 | 7.65 | 6.24 |
| JG35 | 511.1 | 332 | 19.78 | 8.08 | 19.5 | 17.58 | 7.35 | 6.29 |
| JG36 (JRBSD) | 750 | 487 | 20.39 | 7.78 | 64.2 | 16.61 | 7.33 | 6.34 |
| JG37 | 761.2 | 495 | 20.56 | 7.58 | 65.9 | 16.73 | 7.36 | 6.39 |
| JG38 | 779.4 | 507 | 20.39 | 7.69 | 90.3 | 24.77 | 7.45 | 6.44 |
| JG39 | 789.6 | 513 | 20.83 | 7.43 | 83.2 | 23.56 | 7.34 | 6.49 |
| JG40 | 807.5 | 525 | 20.50 | 7.88 | 137.9 | 108.61 | 6.97 | 6.54 |
| JG41 | 802.9 | 522 | 20.44 | 7.86 | 139.6 | 95.32 | 7.03 | 6.59 |
| JG42 | 802.1 | 521 | 20.44 | 7.86 | 139.8 | 86.43 | 7.04 | 6.79 |
| JG43 | 803.6 | 522 | 21.06 | 7.71 | 166.3 | 24.53 | 7.43 | 6.99 |
| JG44 | 803.9 | 523 | 21.11 | 7.76 | 161.3 | 30.4 | 7.42 | 7 |
| JG45 | 808.2 | 525 | 21.78 | 7.97 | 135.7 | 17.78 | 7.41 | 7.19 |
| JG46 | 791.1 | 514 | 21.94 | 7.95 | 176.1 | 17.71 | 7.32 | 7.39 |
| JG47 | 804.5 | 523 | 22.17 | 7.96 | 174.7 | 108.49 | 7.24 | 7.59 |
| JG48 | 800.5 | 520 | 23.06 | 8.03 | 167.4 | 26.03 | 6.96 | 7.79 |
| JG49 | 809.1 | 526 | 22.61 | 7.97 | 178.9 | 37.93 | 7.17 | 7.99 |
| JG50 | 807.8 | 525 | 22.89 | 7.98 | 187.9 | 23.19 | 7.18 | 8 |
| JG51 | 807.4 | 525 | 22.89 | 7.93 | 191.9 | 25.36 | 7.19 | 8.19 |
| JG52 | 809.9 | 526 | 22.78 | 7.94 | 190.1 | 22.52 | 7.17 | 8.39 |
| JG53 | 809 | 526 | 22.83 | 7.93 | 190.2 | 22.45 | 7.2 | 8.49 |
| JG54 | 805.4 | 524 | 23.28 | 8.01 | 182.7 | 20 | 7.12 | 8.54 |
| JG55 | 838.6 | 545 | 24.06 | 7.93 | 176.7 | 20.18 | 7.03 | 8.59 |
| JG56 | 840.1 | 546 | 24.06 | 7.88 | 179.2 | 24.27 | 6.92 | 8.64 |
| JG58 | 843.6 | 548 | 24.11 | 7.83 | 181.4 | 22.02 | 6.94 | 8.69 |
| JG59 | 917 | 596 | 24.56 | 7.8 | 181.7 | 21.07 | 7.07 | 8.74 |
| JG60 (JRJS) | 912.7 | 593 | 24.72 | 7.74 | 181.2 | 22.16 | 6.96 | 8.76 |
| JG61 | 929.3 | 604 | 25.06 | 7.71 | 187 | 21.29 | 6.93 | 8.79 |
| JG62 | 953.2 | 620 | 25.28 | 7.73 | 175.7 | 24.15 | 6.87 | 8.84 |
| JG63 | 972.6 | 632 | 25.56 | 7.67 | 171.1 | 30.74 | 6.9 | 8.89 |
| JG64 | 960.9 | 625 | 25.28 | 7.68 | 178.3 | 25.38 | 6.96 | 8.94 |
| JG65 | 960.9 | 625 | 25.33 | 7.64 | 186.2 | 29.36 | 6.99 | 9 |
| JG68 | 959.5 | 624 | 25.44 | 7.63 | 189.6 | 27.26 | 6.88 | 12 |
| JG69 | 999.1 | 649 | 24.94 | 8.27 | 157.9 | 23.01 | 6.95 | 13 |
| JG70 | 997.5 | 648 | 24.89 | 8.3 | 164.1 | 22.9 | 6.99 | 14 |
| JG71 | 997.9 | 649 | 24.89 | 8.32 | 165 | 22.6 | 6.97 | 14.79 |
| JG72 | 1004.2 | 653 | 25.39 | 8.4 | 153.9 | 25.99 | 7.01 | 14.84 |
| JG73 | 1006.1 | 654 | 25.33 | 8.43 | 160.7 | 24.99 | 6.83 | 14.89 |
| JG74 (JRSQ) | 1008.4 | 655 | 25.39 | 8.43 | 164.1 | 25 | 6.9 | 14.94 |
| JG75 | 1010.2 | 657 | 25.39 | 8.44 | 167.5 | 24.97 | 6.83 | 14.99 |
| JG76 | 1009.4 | 656 | 25.44 | 8.42 | 164.1 | 24.95 | 6.83 | 15 |
| JG77 | 1007 | 655 | 25.44 | 8.4 | 164.4 | 26 | 6.88 | 15.04 |
| JG78 | 1009.4 | 656 | 25.39 | 8.43 | 165.6 | 25.76 | 6.81 | 16 |
| JG79 | 989.3 | 643 | 26.50 | 8.51 | 138.1 | 44.68 | 6.93 | 17 |
| JG80 | 989.6 | 643 | 26.44 | 8.53 | 146.7 | 32.43 | 6.75 | 18 |
| JG81 | 991.2 | 644 | 26.06 | 8.49 | 157.2 | 32.72 | 6.99 | 19 |
| JG82 | 995 | 647 | 25.94 | 8.52 | 158.7 | 32.46 | 6.97 | 20 |
| JG83 | 991.3 | 644 | 26.06 | 8.52 | 159.6 | 32.27 | 6.9 | 21 |
| JG93 | 984.6 | 640 | 26.17 | 8.49 | 178.5 | 34.73 | 6.89 | 22.33 |
| JG92 | 985.6 | 641 | 26.17 | 8.54 | 181.1 | 36.61 | 6.89 | 22.38 |
| JG91 | 986.7 | 641 | 26.06 | 8.53 | 177.8 | 34.31 | 6.93 | 22.43 |
| JG90 (JRAG) | 987.5 | 642 | 26.06 | 8.5 | 174.4 | 33.52 | 7.02 | 22.48 |
| JG89 | 899.6 | 585 | 26.17 | 8.51 | 169.9 | 35.06 | 6.78 | 22.53 |
| JG88 | 896.2 | 583 | 26.06 | 8.43 | 169.6 | 32.05 | 6.93 | 22.58 |
| JG87 (JRBG) | 849.7 | 552 | 26.22 | 8.5 | 173.9 | 34.92 | 6.76 | 22.63 |
| JG86 | 849.9 | 552 | 26.17 | 8.5 | 171 | 35.84 | 6.79 | 22.68 |
| JG98 (SY) | 1252.3 | 814 | 27.39 | 8.15 | 175.7 | 60.03 | 7.17 | 37 |